This section provides complete details of the experimental results and subsequent analysis performed to determine the kinetic model and its parametersfor the palladium-based catalysts.

Experimental Reactor

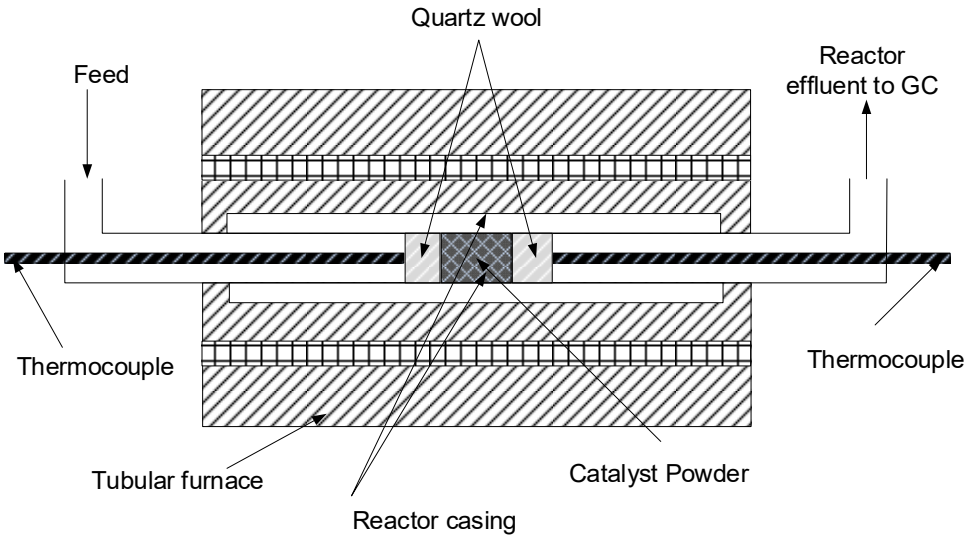

Figure S1 – Schematic of the experimental reactor and furnace.

Ignition curves – dry runs on fresh catalyst 1.

Ignition curves were obtained on the fresh catalyst at inlet methane concentrations of 1000, 2000, 3000 and 5000 ppm. One wet run was also performed with 5000 ppm methane. The results are shown in Figure S2. For the first runs performed at 1000 ppm methane after calcining there was some fluctuation in activity. The first run (not shown) exhibited relatively low activity, which behavior has been observed previously over other catalysts. The second ignition curve was higher and then the curves were reproducible.

For comparison purposes, the dry runs are shown together in Figure S3. There is a systematic dependence of the conversion on the methane concentration. This effect is indicative of inhibition by water produced by combustion.

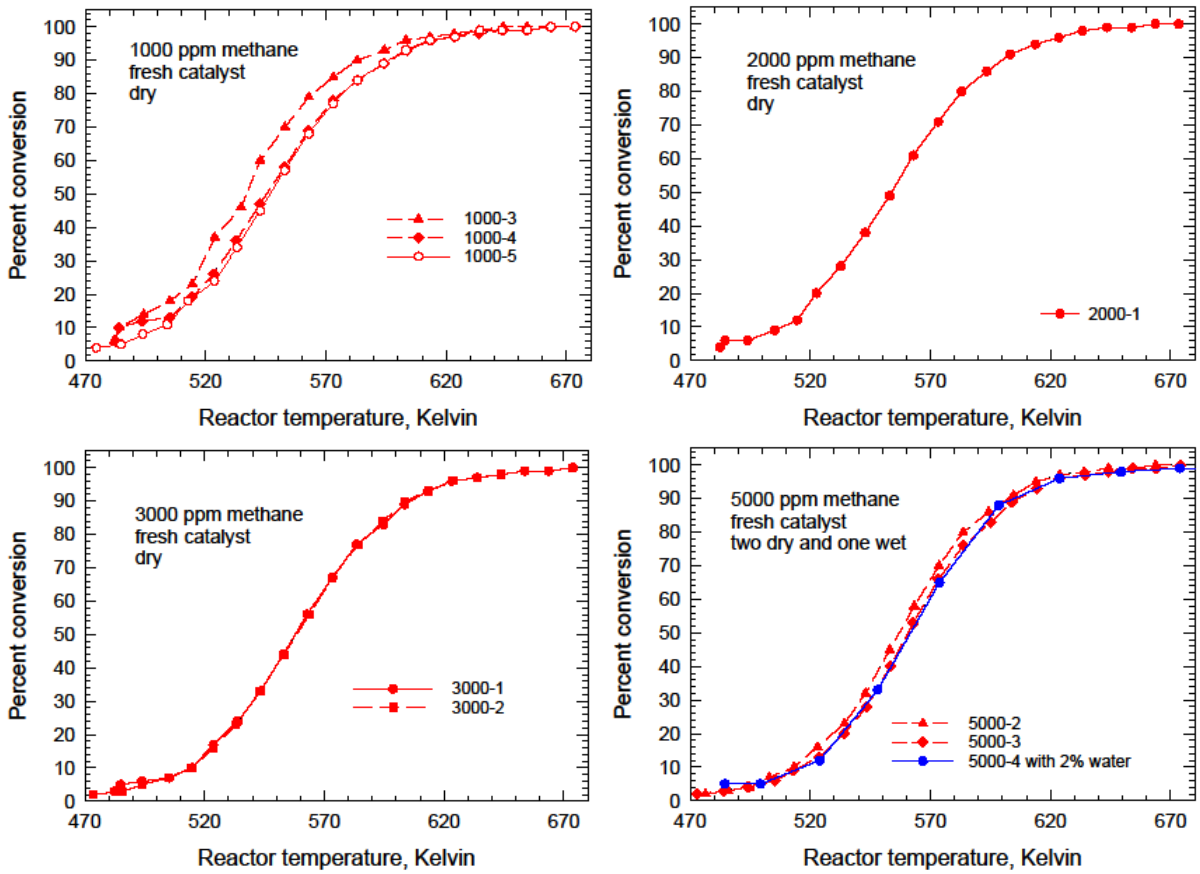

Figure S2 – Ignition curves on fresh Catalyst 1 for runs without water with 1000, 2000, 3000 and 5000 ppm methane. One run was done with 2 % water at 5000 ppm methane. The symbols represent experimental points and the lines simply connect the symbols as an aid to the eye.

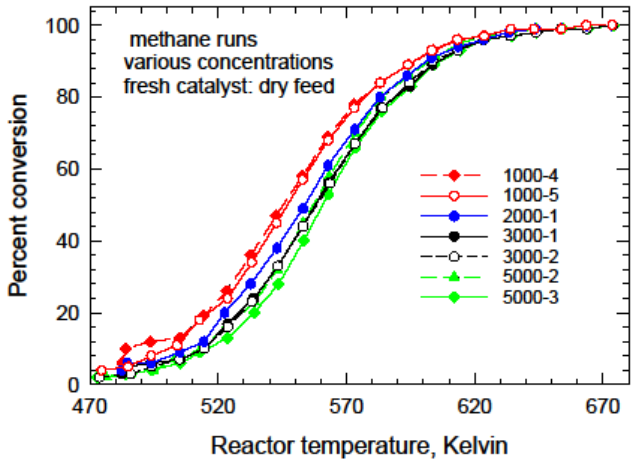

Figure S3 – Comparison of the ignition curves obtained under dry conditions. There is a dependence on methane concentration, which indicates an inhibition effect of water. Catalyst 1

Hydrothermal ageing – First set, Catalyst 1

After the dry ignition experiments, the catalyst was hydrothermally aged (HTA-1) for 72 hours at the same overall flow rate of 210 ml/min (STP dry basis) with 5000 ppm methane and 2 % water vapour. The temperature was 450 ℃, with the temperature being lowered periodically to 285 ℃ to measure the low temperature activity. The activity over time at 285 ℃ is shown in Figure S4. Each point represents the average of four measurements. The conversion at 450 ℃ remained at 100 % for the entire ageing process. The activity decreases by about 50 % over the 72 hours.

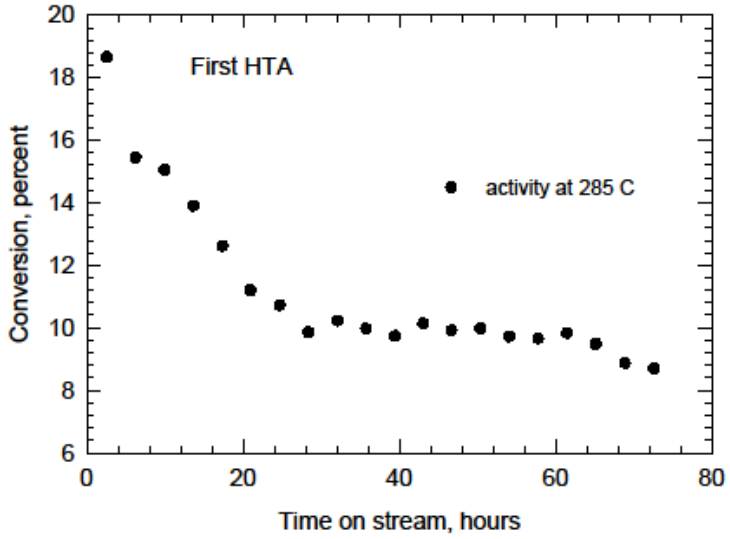

Figure S4 – Conversion at 285 ℃ during the first experiment on hydrothermal ageing. The ageing occurred at 450 ℃. Catalyst 1.

Following HTA-1, a set of ignition curves was measured in the absence of water. The first three runs were performed at 5000 ppm methane. The first result showed a low activity compared to the next two, the latter being very reproducible. The ignition curves are shown in Figure S5, with the results for the fresh catalyst also shown for comparison. The experiments at 5000 were followed by two runs at 1000 ppm methane and one at 3000 ppm, all without water. These curves are also shown in Figure S5. Compared to the dry activity before the HTA, the activity is noticeably lower.

After finishing these five ignition curves, the laboratory was required to be vacated for six weeks. During this time, the reactor was shut down and the catalyst left in situ at room temperature. After resumption, the catalyst was heated to 450 ℃ in air and then cooled. Ignition curves were then obtained at 1000, 2000, 3000 and 5000 ppm methane. Figure S6 shows comparisons of the ignition curves obtained for the fresh catalyst, the catalyst immediately after HTA-1, and the catalyst after resting for six weeks. It was observed

that the activity for each of these concentrations after the six-week rest had almost fully recovered to the level observed prior to the HTA. We have observed that activity of Pd catalysts can recover somewhat after HTA when exposed to dry reacting mixtures, but we have never testing over such a long time period.

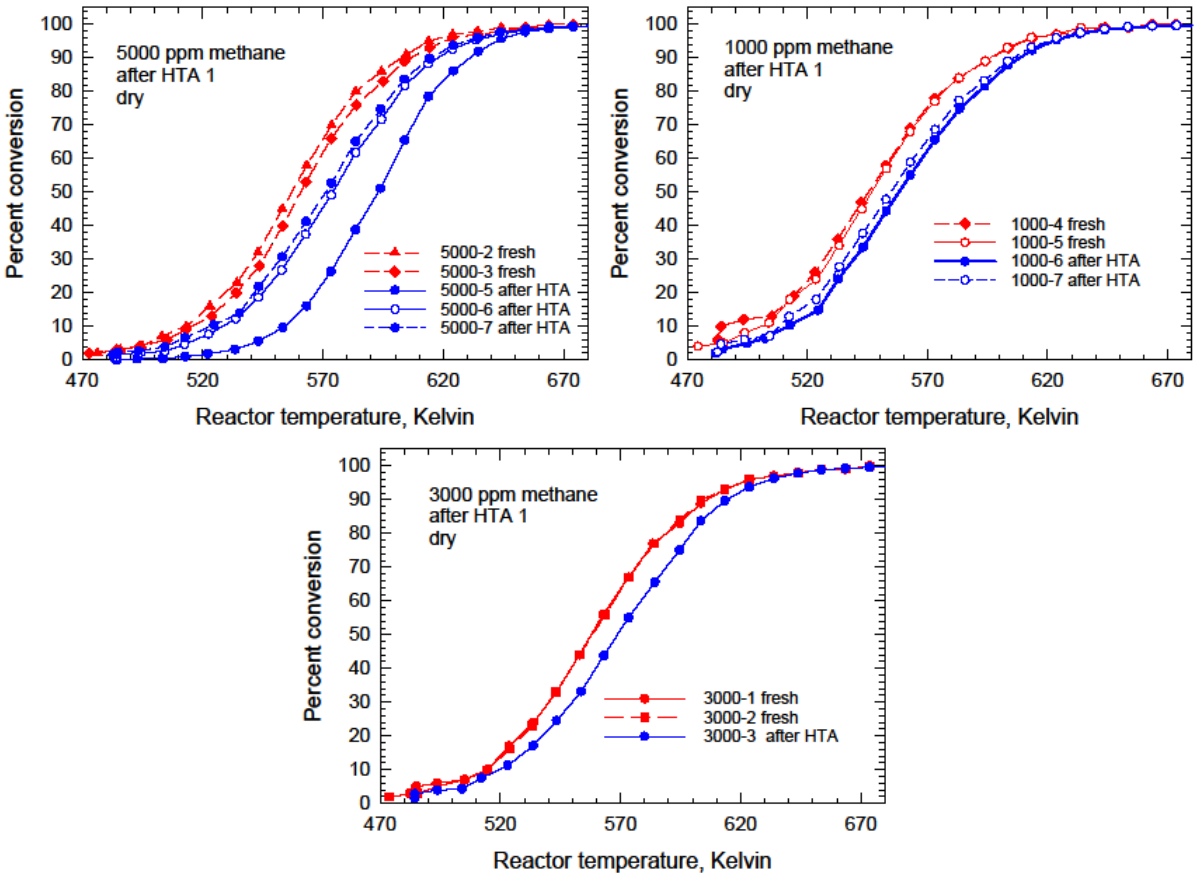

Figure S5 – Ignition curves under dry conditions obtained after 72 hours of hydrothermal ageing at 450 ℃. The activity of the HTA catalyst is noticeably lower. Catalyst 1

It is clear that there is a change in activity after the HTA if the catalyst is no longer exposed to water. Because the interest in these experiments was to evaluate the catalyst under wet conditions after ageing, a new HTA was performed followed immediately by the measurement of a set of ignition curves under wet conditions. The second HTA was carried out at 550 ℃ for 72 hours. The activity at 355 ℃ was periodically measured during this HTA experiment. The decline in activity is shown in Figure S7. The activity may still be declining at 72 hours.

After 72 hours of HTA the reactor was cooled and a series of ignition curve experiments was performed with 2 % water present. Runs were first performed with 5000 ppm methane, followed by runs at 3000 and 1000 ppm. All of these runs showed essentially the same ignition curve, indicating apparent first order behaviour. A set of dry runs was then performed in the order 5000, 3000, 1000 and then a repeat of 5000. The two runs at 5000 ppm methane were essentially the same, showing that there had been negligible catalyst reactivation between the two runs at 5000.

We can compare the dry activities for the fresh catalyst with those after HTA-1 and HTA-2. Figure S9 compares the activity of the ignition curves for 5000 ppm methane. It is seen that the activity of the dry ignition curve is similar to the first curve measured after HTA-1 under dry conditions. Generally, the dry curves after HTA-2 are lower than those measured after HTA-1 (and before the six-week rest).

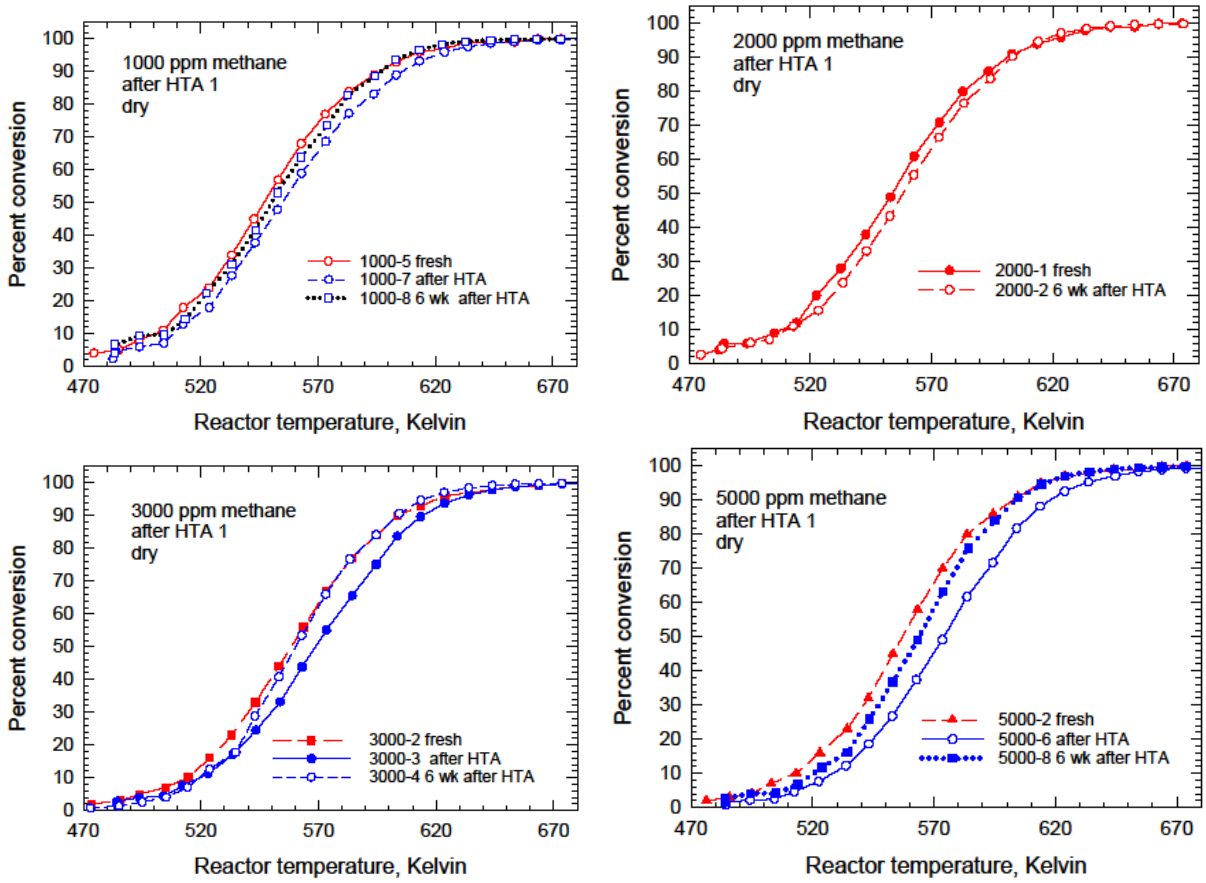

Figure S6 – Ignition curves under dry conditions obtained after 72 hours of hydrothermal ageing at 450 ℃. The results after six weeks of shutdown are shown. A considerable recovery in activity is observed. Catalyst 1

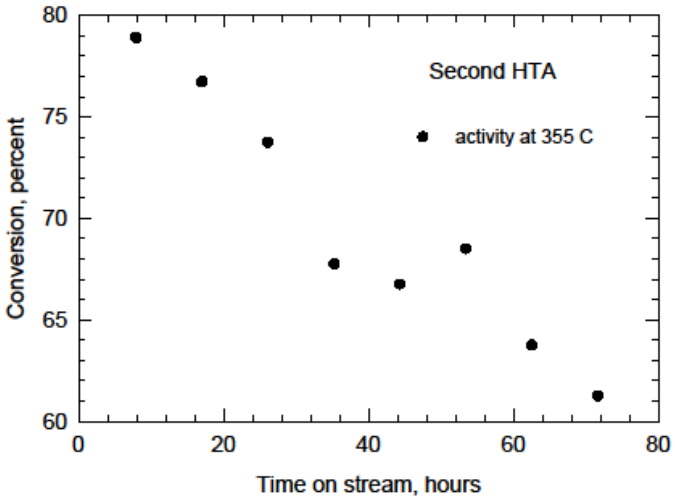

Figure S7 - Conversion at 355 ℃ during the first experiment on hydrothermal ageing. The ageing occurred at 550 ℃. Catalyst 1

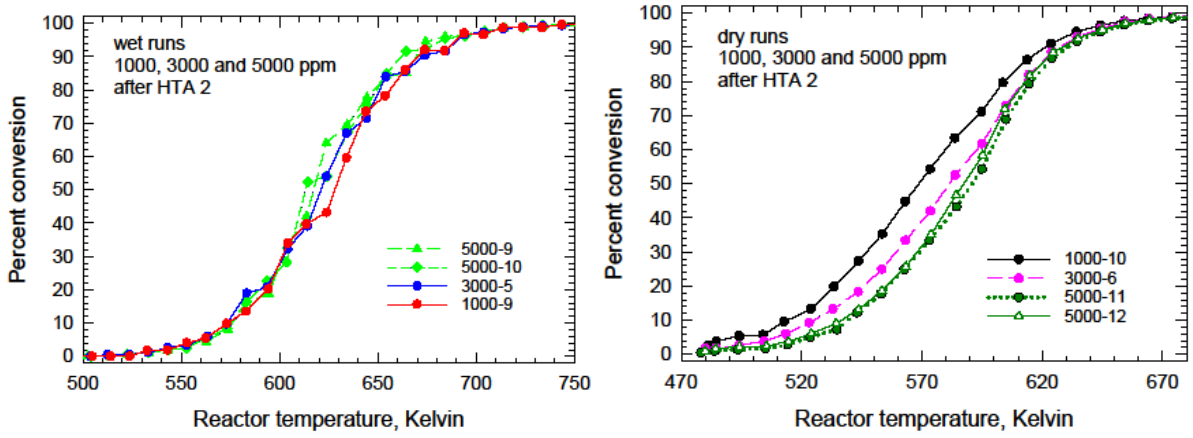

Figure S8 – Wet (left) and dry (right) ignition curves after HTA number 2. The wet runs were performed first and all curves were essentially the same. The dry runs were performed in the order 5000, 3000 1000 and then 5000 again. Catalyst 1

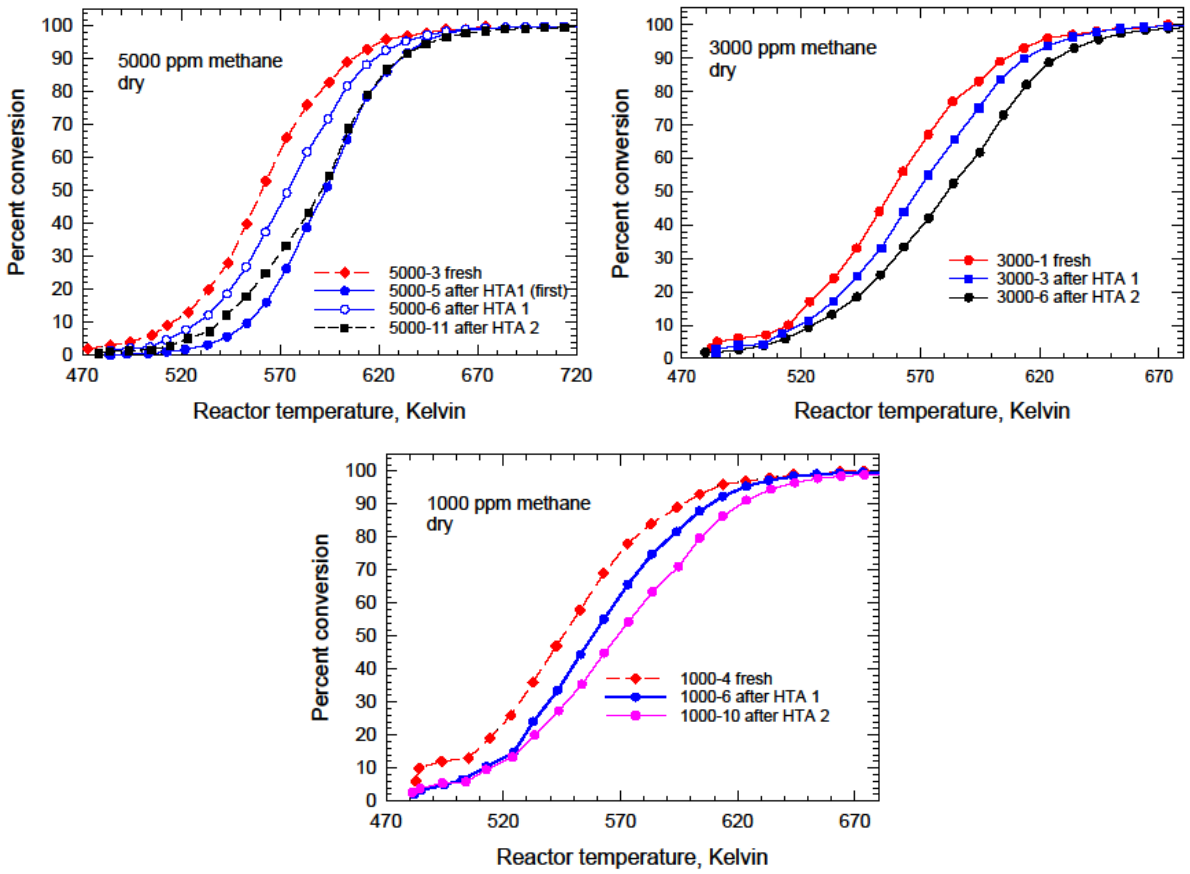

Figure S9 – Comparison of the dry activities after HTA-2 to the fresh and HTA-1 catalysts. For 5000 ppm the activity is similar to the first curve for 5000 ppm methane measured immediately after HTA-1. For 3000 and 1000 ppm the dry activity after HTA-2 is lower than that observed after HTA-1. Catalyst 1

Following the dry runs after HTA-2, the catalyst was again hydrothermally aged at 640 ℃. The activity was measured intermittently at 355 ℃. The plot of this latter activity with time is shown in Figure 10. Each point represents the average of four conversion measurements.

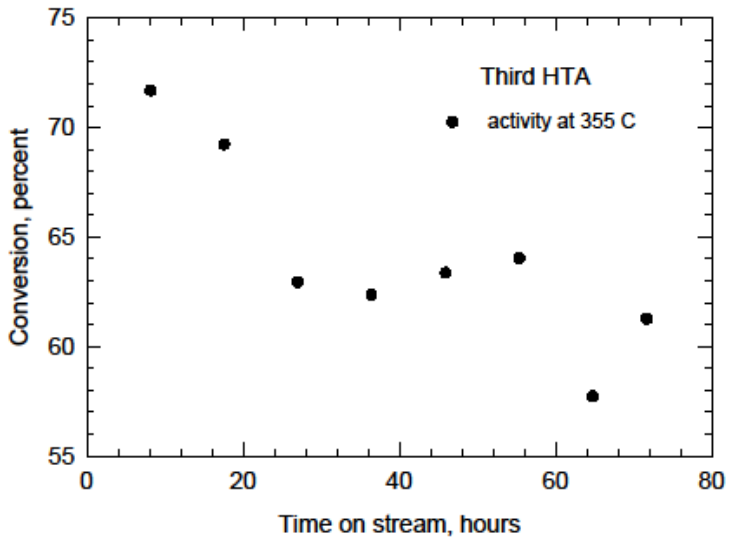

Figure S10 - Conversion at 355 ℃ during the third experiment on hydrothermal ageing. The ageing occurred at 640 ℃. Catalyst 1

After the end of HTA-3 test, two, ignition curves were taken in wet conditions (2% water present) at 1000 and 5000 ppm methane. The two curves were essentially coincident as shown in Figure S11. After the wet runs, a series of dry runs was performed, with the results shown also in Figure S11. The dry runs were performed in the order 5000, 1000 and then 5000 again. The reproducibility of the 5000 ppm methane curves indicates that the catalyst activity was stable during these experiments.

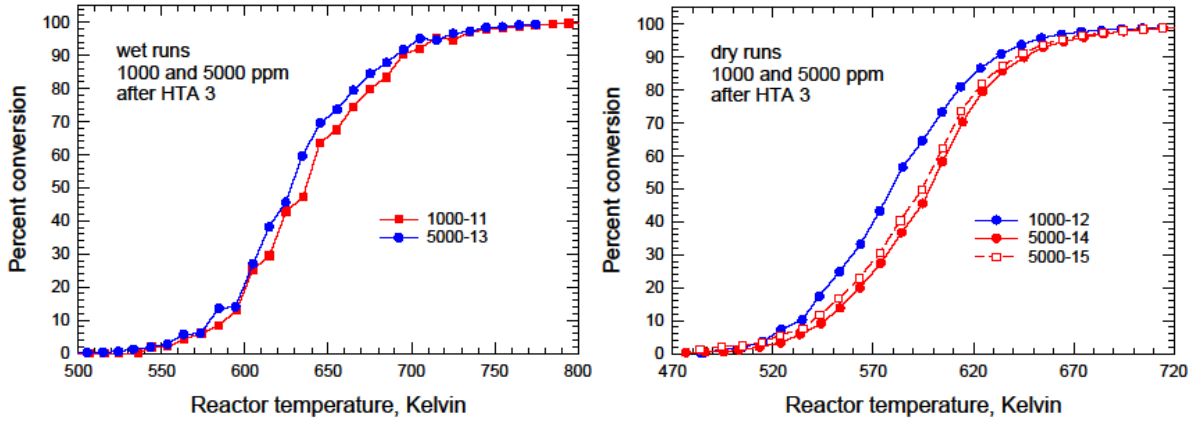

Figure S11 – Wet (left) and dry (right) ignition curves after HTA-3 The wet runs were performed first and all curves were essentially the same. The dry runs were performed in the order 5000, 1000 and then 5000 again. Catalyst 1

Figure S12 shows some comparisons of activities at different treatment levels. Expanding on Figure 9, the dry activities after HTA-3 for 1000 and 5000 ppm methane are added.

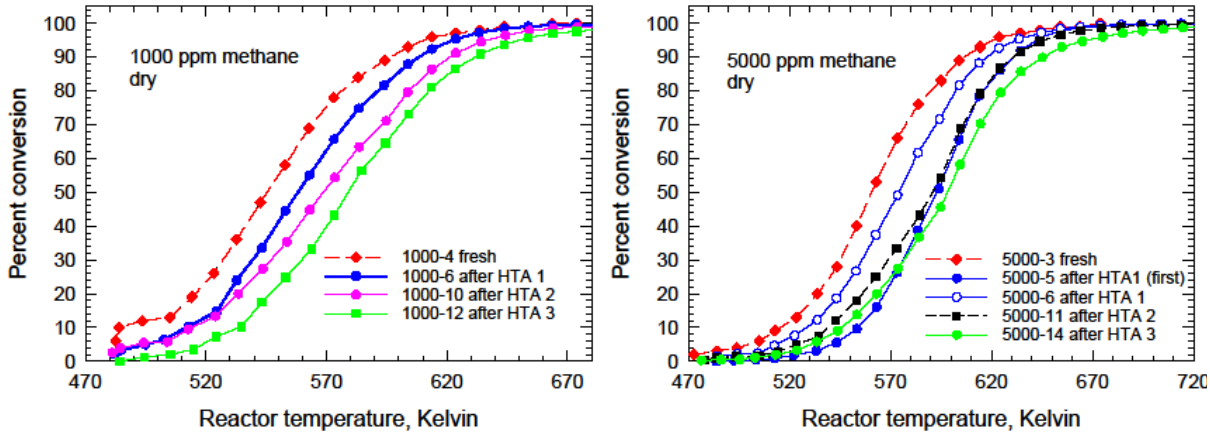

Figure S12 – Activity with dry feed for 1000 and 5000 ppm methane for fresh catalyst, compared to activity after the three HTA runs. For the HTA-1, the conversion curves are those measured before the six-week rest. Catalyst 1

After the completion of the dry tests, the catalyst was held for 60 hours at a constant temperature of 350 ℃ (623 K) under dry conditions with 5000 ppm methane. The conversion showed a slow decrease during this time to give a final conversion of the order of 73 %. The ignition curve experiments are summarized in Table S1.

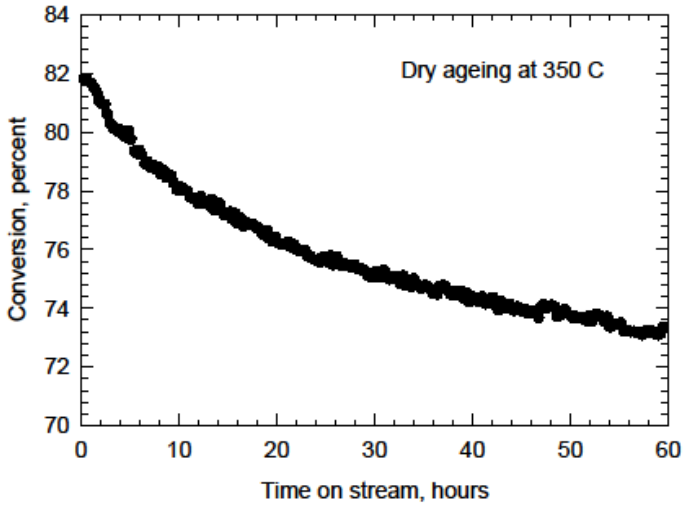

Figure S13 – Activity under dry feed with 5000 ppm methane after all of the testing was complete. There is a slow decline in activity. Catalyst 1

Table S1 – Summary of ignition curves and conditions for Catalyst 1.

Run number	Methane concentration ppmv	Wet or dry	Catalyst History
1000-3	1000	dry	Fresh catalyst after calcination
1000-4	1000	dry	
1000-5	1000	dry	
2000-1	2000	dry	
3000-1	3000	dry	
3000-2	3000	dry	
5000-2	5000	dry	
5000-3	5000	dry	
5000-4	5000	2 % water	
1000-6	1000	dry	Immediately after HTA-1
1000-7	1000	dry	
3000-4	3000	dry	
5000-5	5000	dry	
5000-6	5000	dry	
5000-7	5000	dry	
1000-8	1000	dry	After HTA-1 and 6 weeks rest
2000-2	2000	dry	
3000-4	3000	dry	
5000-8	5000	dry	
5000-9	5000	2 % water	Immediately after HTA-2
5000-10	5000	2 % water	
3000-5	3000	2 % water	
1000-9	1000	2 % water	
1000-10	1000	dry	After HTA-2 and the wet runs
3000-6	3000	dry	
5000-11	5000	dry	
5000-12	5000	dry	
5000-13	5000	2 % water	Immediately after HTA-3
1000-11	1000	2 % water	
5000-14	5000	dry	After HTA-3 and the wet runs
1000-12	1000	dry	
5000-15	5000	dry	

Ignition curves – dry runs on fresh catalysts 2 to 6.

Figures S14 to S18 show the ignition curves obtained for the catalysts 2 to 6 under dry feed conditions with fresh catalyst. In most cases, either 2 or 3 runs were performed. For Catalyst 2 it was seen that the first run at each concentration showed conversions higher than for runs 2 and 3. For the other catalyst, the repeat runs were consistent.

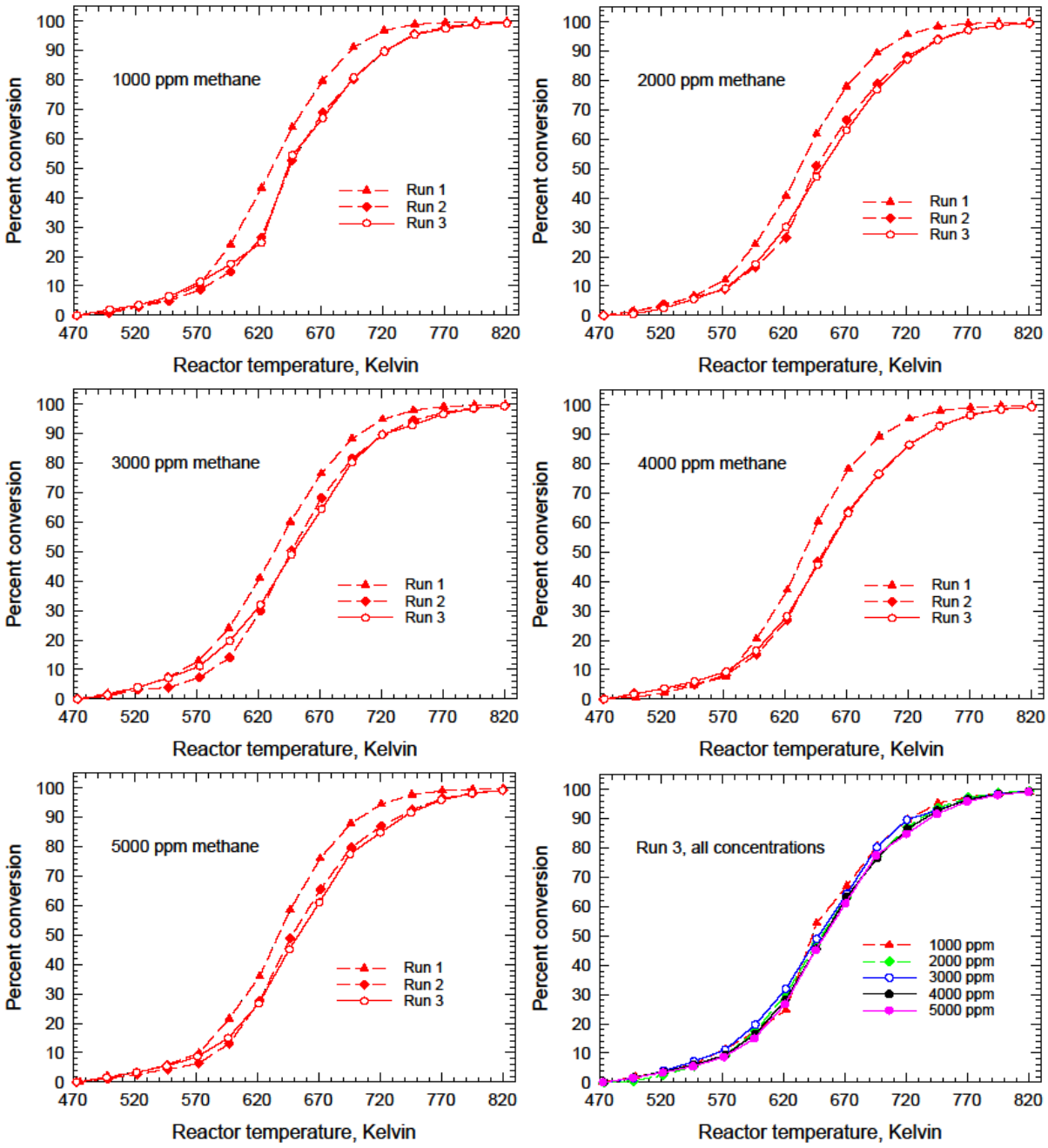

Figure S14 - Ignition curves for Catalyst 2, Pd:Pt supported on Co_3O_4/SnO_2.

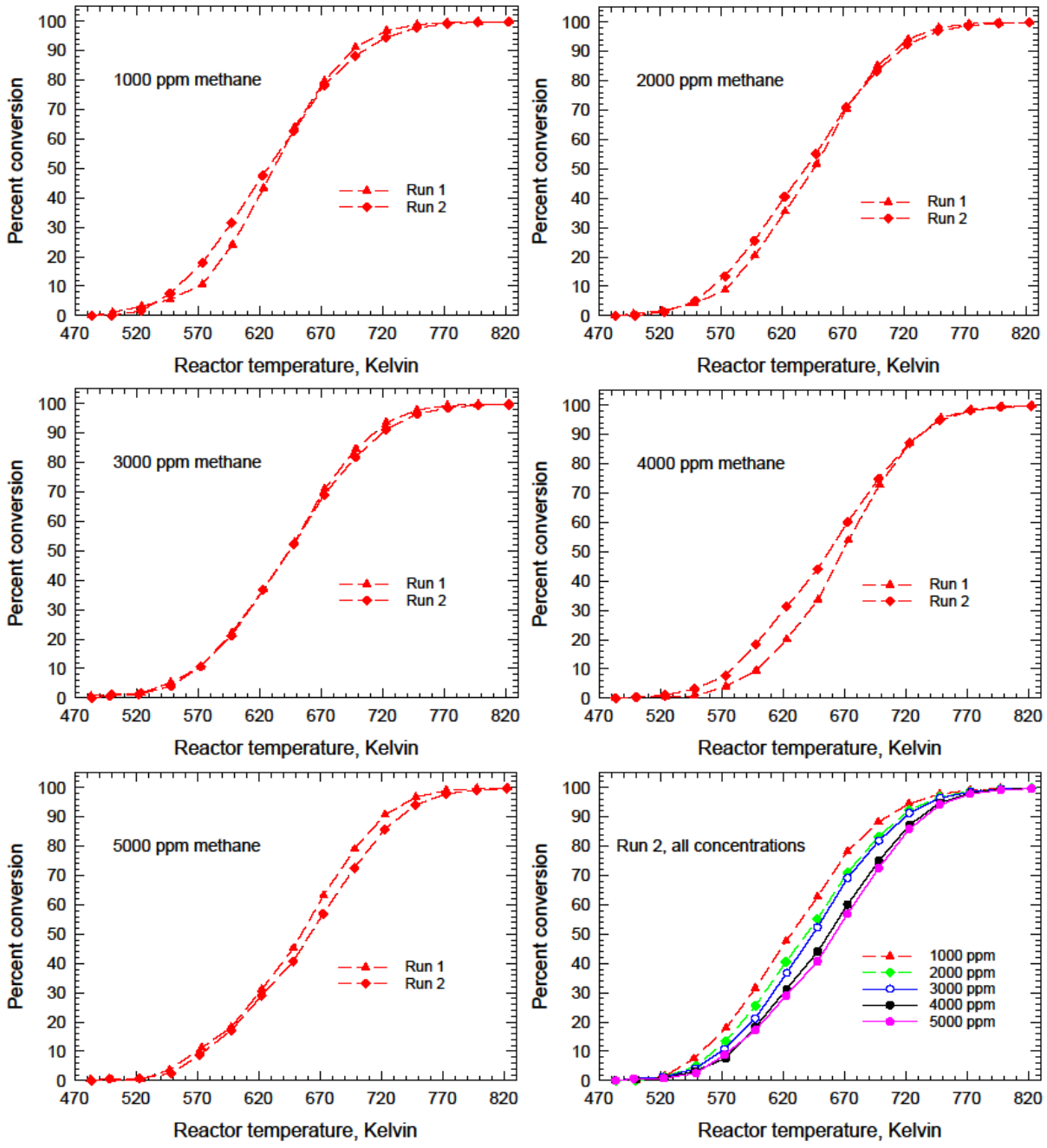

Figure S15 - Ignition curves for Catalyst 3, Pd:Pt supported on SnO_2.

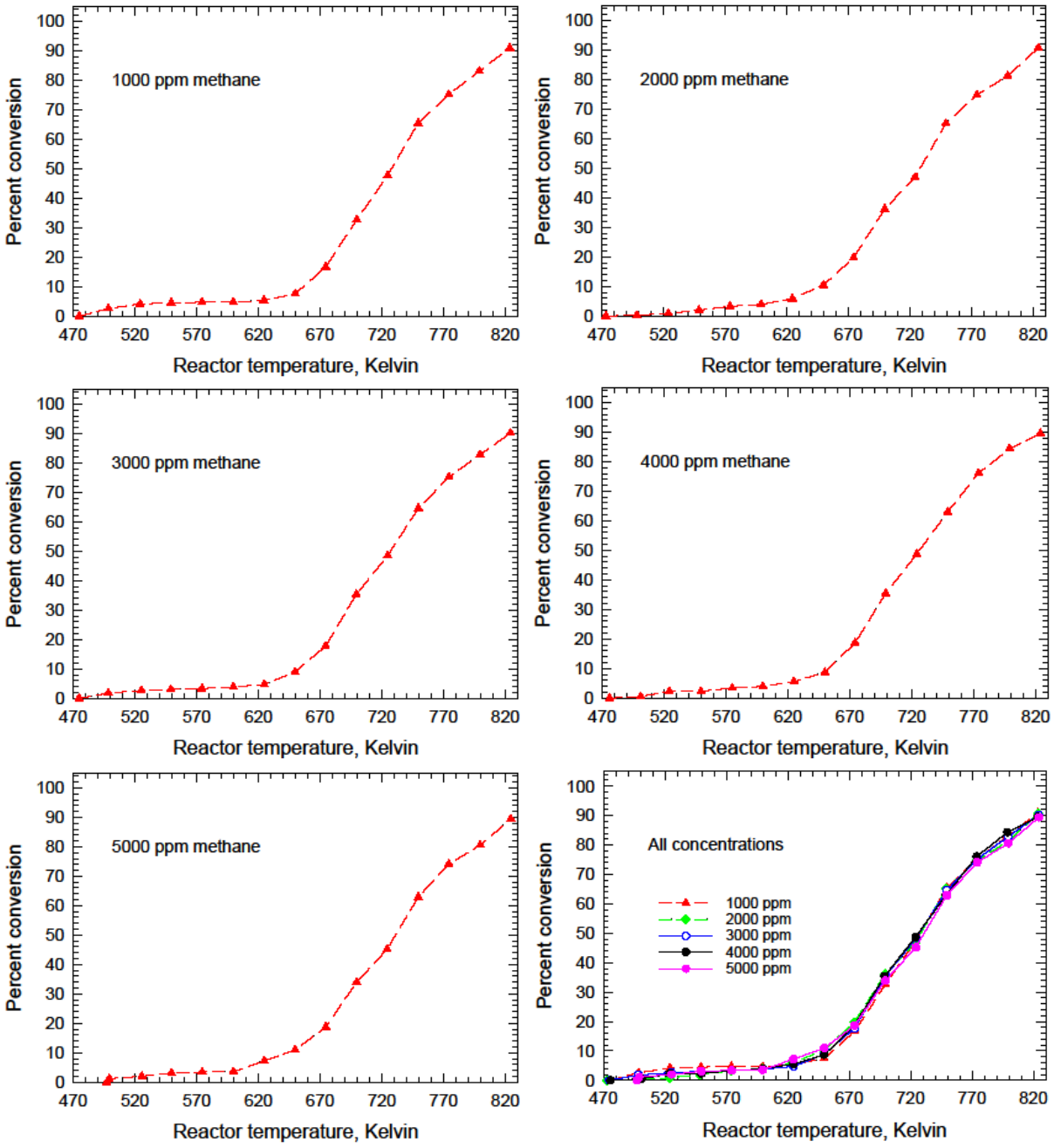

Figure S16 - Ignition curves for Catalyst 4, Pd:Pt supported on Co_3O_4 .

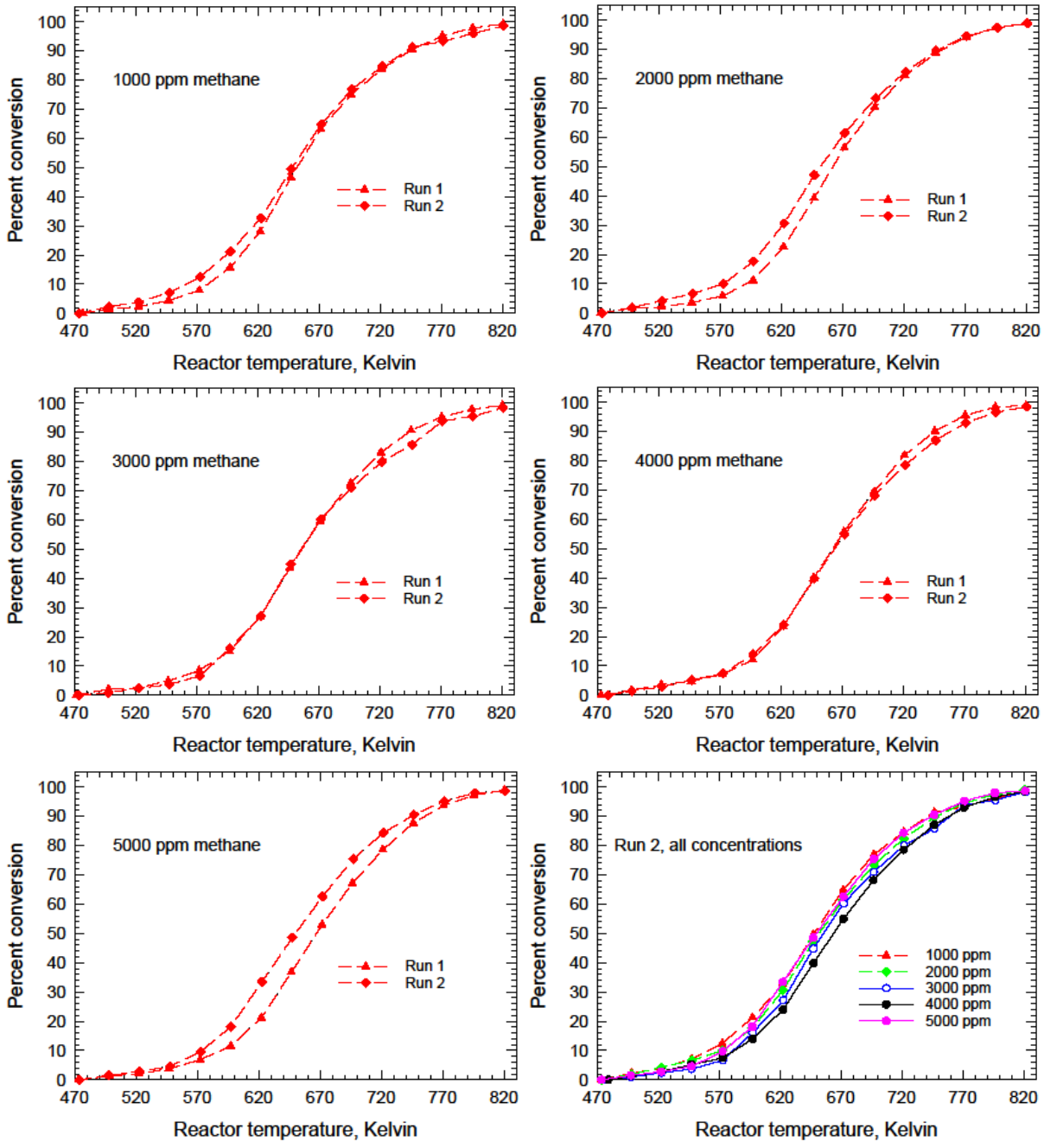

Figure S17 - Ignition curves for Catalyst 5 Pd:Pt supported on $Co_3O_4/\gamma\text{-}Al_2O_3$.

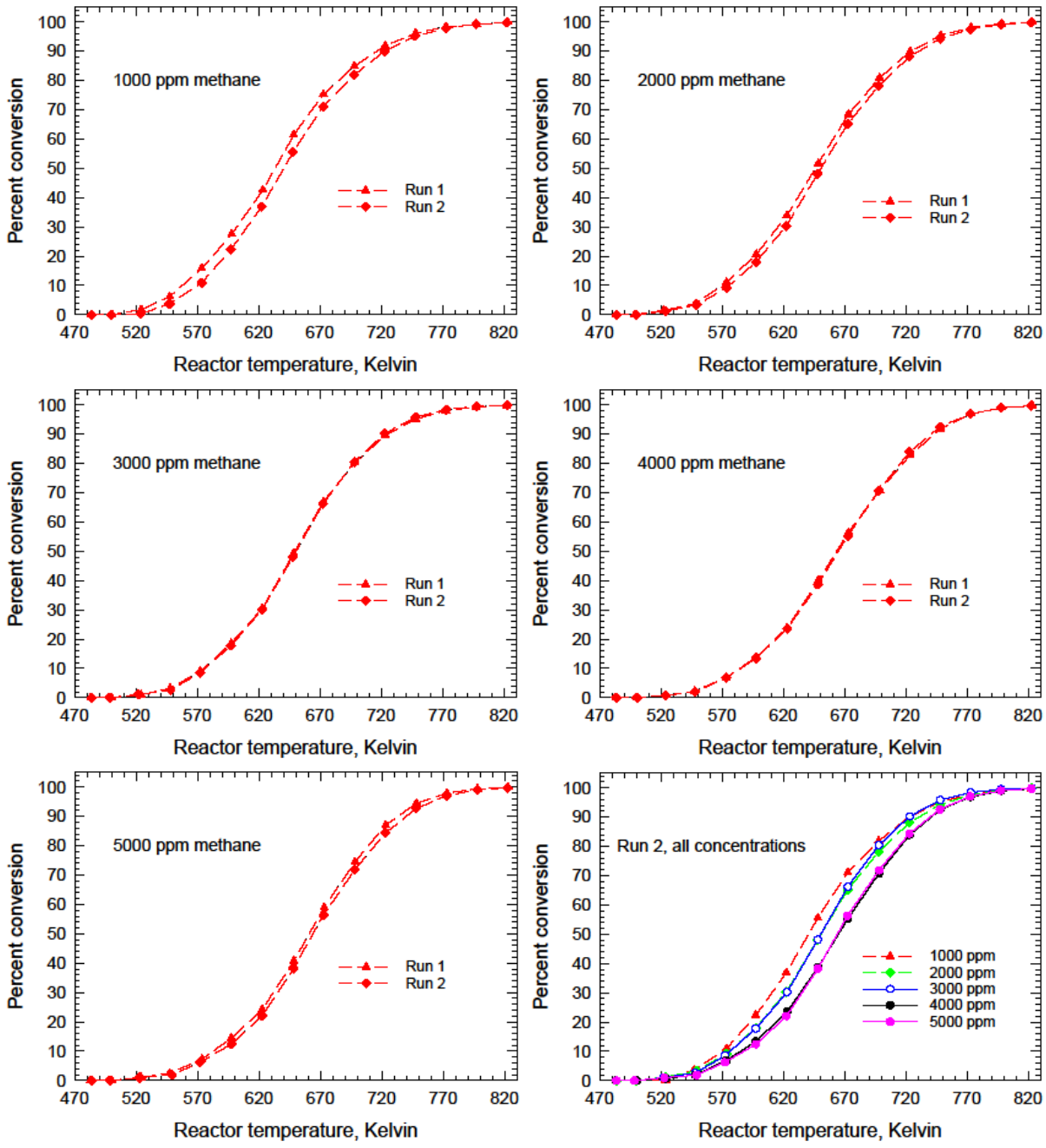

Figure S18 - Ignition curves for Catalyst 6 Pd:Pt supported on γ-Al_2O_3

Kinetic modelling sections

Arrhenius plots – first order reaction for Catalyst 1

As a first step in analyzing the results, we use a simple first order reaction in terms of methane, and then determine the apparent activation energy and pre-exponential factors at each concentration value. We assume plug flow in the reactor, and analyze the results at a constant temperature, using the average of the two thermocouples in the bed. In terms of total catalyst mass, the mole balance in the plug flow reactor is written as:

$$-\frac{dF_A}{dW} = (-r_A) = k\,C_A = k\frac{F_A}{Q} \tag{S1}$$

In Equation (1), W is the total mass of ground catalyst (washcoat and substrate) and Q is the volumetric flow rate at the temperature and pressure in the reactor. The equation is expressed in terms of fractional conversion as:

$$F_{A0}\frac{dX_A}{dW} = k\frac{F_{A0}}{Q}(1-X_A) \tag{S2}$$

Equation 2 can be rearranged and integrated analytically to give an explicit expression for the apparent first order rate constant:

$$k = \frac{Q}{W}\int_0^{X_A}\frac{dX_A}{(1-X_A)} = -\frac{Q}{W}\ln(1-X_A) \tag{S3}$$

The value of the apparent rate constant was calculated for every ignition curve using only the data corresponding to conversion between approximately 15 and 85 %. Using simple regression analysis, the Arrhenius equation was fit, according to the following representation:

$$k = \exp\left\{A - E\left(\frac{1000}{R_g T}\right)\right\} \quad \text{or} \quad \ln(k) = A - E\left(\frac{1000}{R_g T}\right) \tag{S4}$$

Where A is a constant factor and E is the activation energy in kJ/mol. The constant A, which is usually referred to as the preexponential factor, was here included in the exponential term. This trick enables a more stable and efficient optimization process.

Arrhenius plots – experiments on the fresh catalyst

The first set of ignition curves analyzed are the (mostly) dry ignition curves obtained prior to the first hydrothermal ageing, HTA-1 for Catalyst 1. Figure S19 shows these Arrhenius plots. For each run, the apparent activation energy is calculated using the data from that run. Where two runs were done at the same concentration of methane, then the results from doing the regression analysis on the data from both runs are also shown. The

results are summarized in Table S2. The main observation is that there is a gradual increase in the apparent activation energy, which is consistent with an activated adsorption term for water which inhibits the reaction.

The conclusion at this point is that a first order model is not appropriate at these water concentrations. The apparent activation energies are also in the same range as observed by others for Pd catalysts in methane combustion.

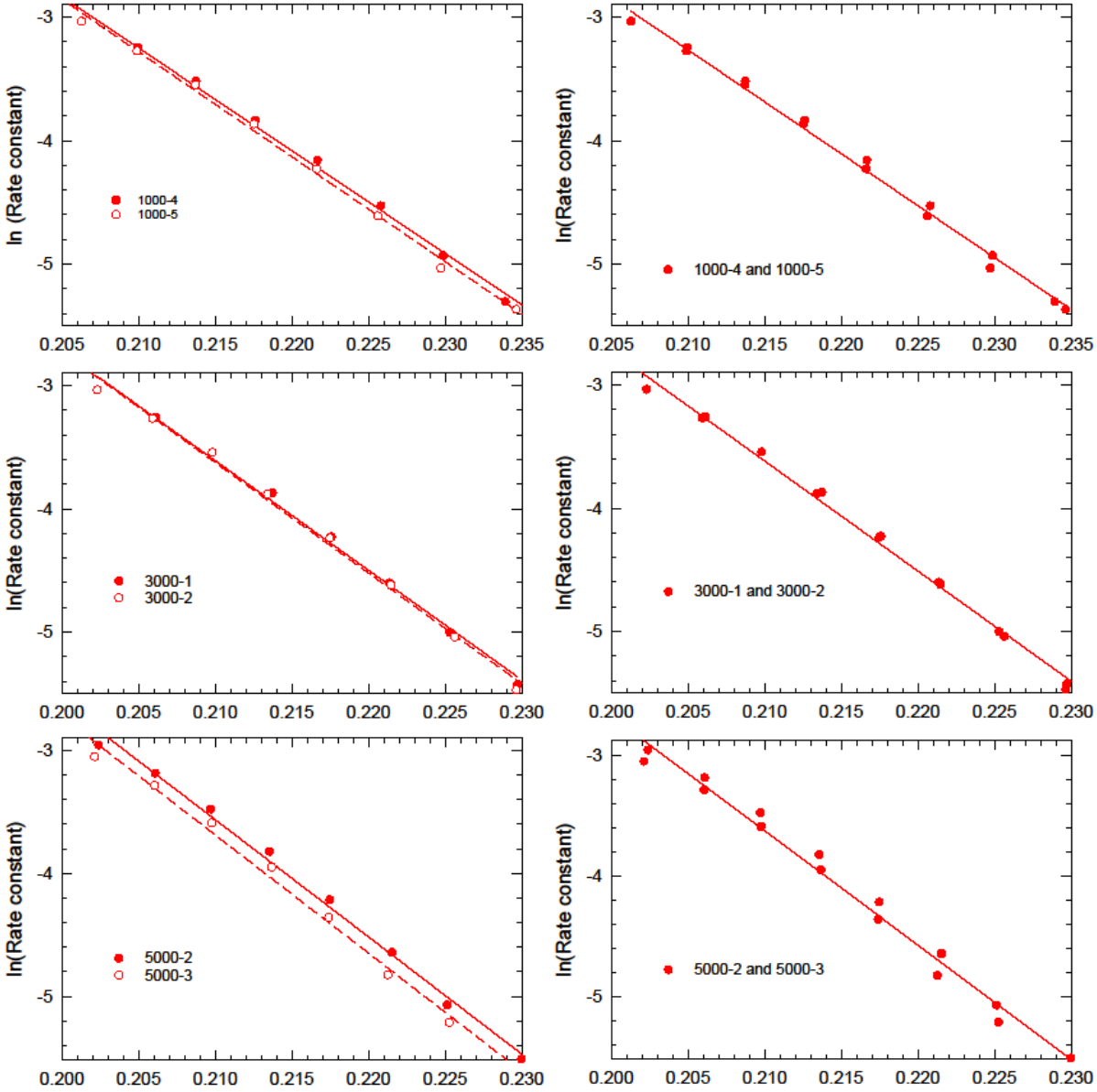

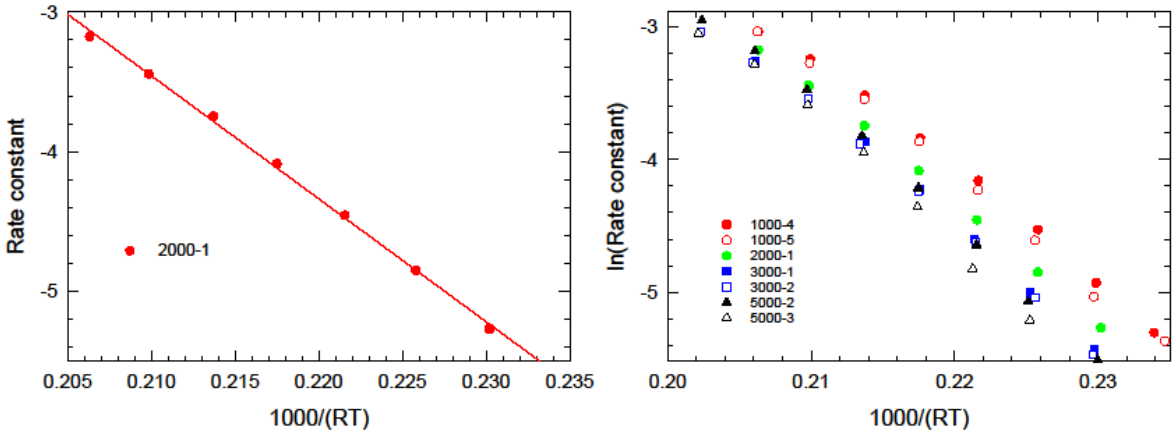

Figure S19 – Arrhenius plots for first order reaction for the dry runs on fresh catalyst. Catalyst 1.

Note: In Table S2, the parameter A is the one obtained from the optimization of the kinetic expression in the form of Equation (S4)

$$k = \exp\left\{A - E\left(\frac{1000}{R_g T}\right)\right\} \quad \text{or} \quad \ln(k) = A - E\left(\frac{1000}{R_g T}\right) \tag{S5}$$

The standard Arrenius equation has the form:

$$k = k_0 \exp\left\{-E\left(\frac{1000}{R_g T}\right)\right\} \quad \text{where} \quad k_0 = \exp\{A\} \tag{S6}$$

Table S2 includes both versions.

Table S2 – Summary of parameters obtained for the dry runs on the fresh catalyst.

Run details	A	k_0	E
1000-4	14.19	1.45E+06	83.06
1000-5	14.56	2.11E+06	84.95
1000-4 and 1000-5	14.38	1.76E+06	84.02

2000-1	15.02	3.34E+06	87.98
3000-1	15.05	3.44E+06	88.87
3000-2	15.21	4.03E+06	89.68
3000-1 and 3000-2	15.13	3.72E+06	89.28
5000-2	16.45	1.39E+07	95.3
5000-3	16.5	1.47E+07	96.11
5000-2 and 5000-3	16.26	1.15E+07	94.69
5000-4 2% water	15.89	7.96E+06	93.35
All dry runs together	14.04	1.25E+06	83.68

First order Arrhenius plots following HTA-1

After the first hydrothermal aging test (HTA-1), a series of dry runs was performed, which was interrupted by a spell during which the catalyst sat for six weeks. As shown in the ignition curves presented earlier in the document, the catalyst activity changed significantly during the six-week rest at room temperature.

The general trend in the apparent activation energies is the same as that observed for the fresh catalyst. That is, the apparent activation energy increases as the methane concentration increases. For the ignition curves measured directly after the HTA, the order of magnitude for the apparent activation energy is the same before and after the HTA, however, the pre-exponential factor is smaller. After the six-week rest, the activities were observed to be higher than before the hiatus.

The graphs are shown in Figure S20 for the results obtained before the six-week hiatus, whilst Figure S21 shows the results obtained after this period. The parameter values are summarized in Table 3.

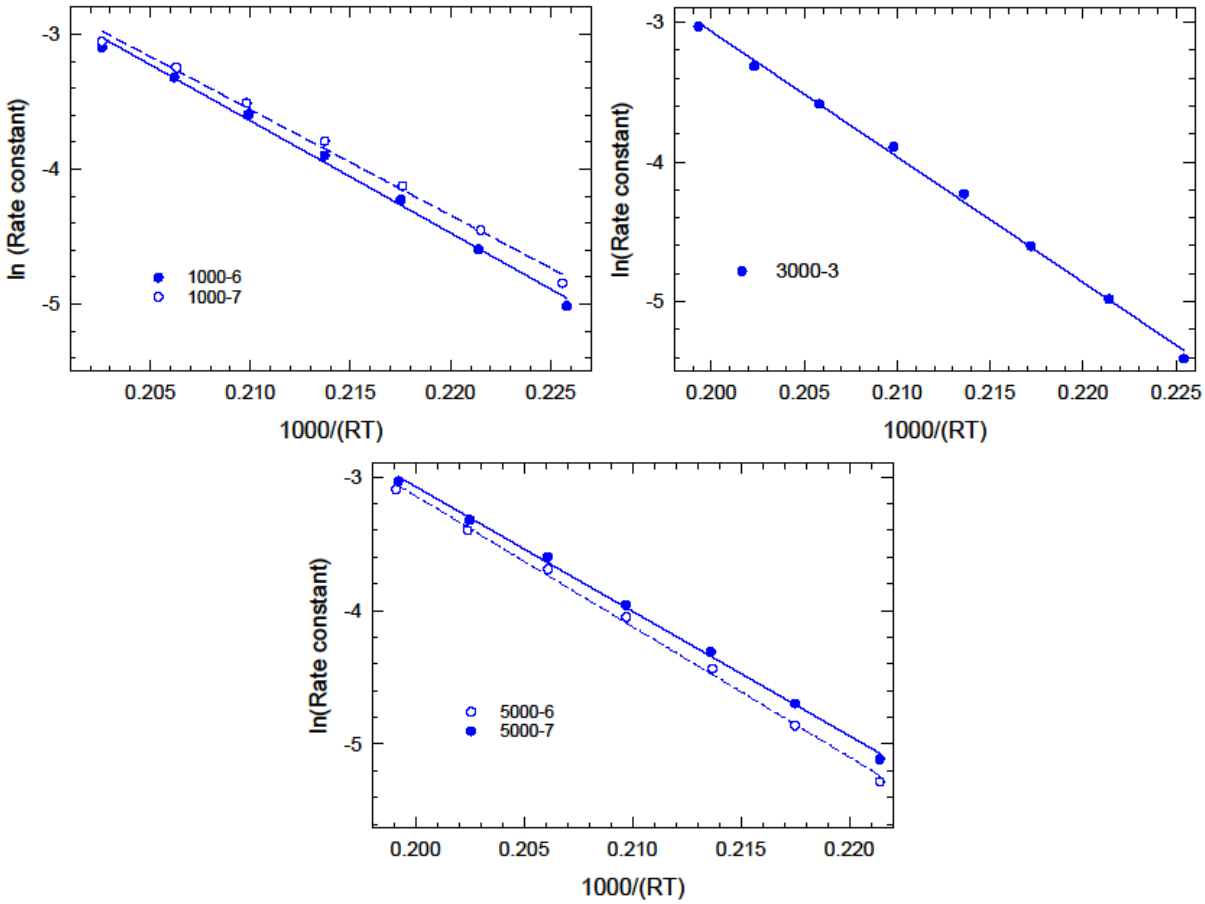

Figure S20 – First order Arrhenius plots for the dry ignition curves obtained after the HTA 1 and before the six-week hiatus.

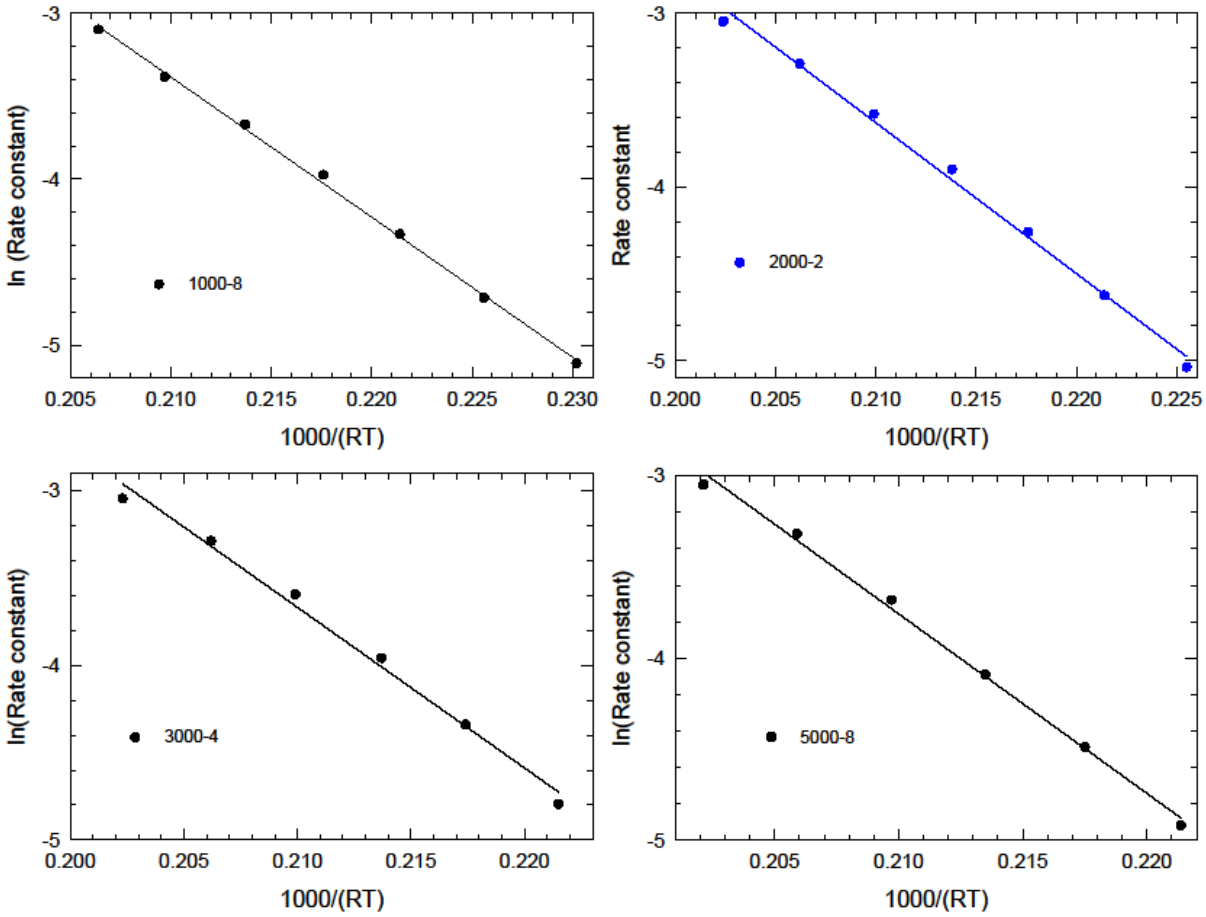

Figure S21 – First order Arrhenius plots for the dry ignition curves obtained after the HTA 1 and after the six-week hiatus.

Table S3 – Summary of parameters obtained for the dry runs on the catalyst following HTA 1.

Run details	*A*	k_0	*E*
1000-6	13.83	1.01E+06	83.20
1000-7	12.91	4.04E+05	78.43
3000-3	14.89	2.93E+06	89.78
5000-6	16.43	1.37E+07	97.83
5000-7	15.57	5.78E+06	93.24
After six weeks rest			
1000-8	14.36	1.72E+06	84.46
2000-2	14.59	2.17E+06	86.78
3000-4	15.67	6.39E+06	92.07
5000-8	16.94	2.27E+07	98.57

First order Arrhenius plots following second hydrothermal ageing

After the second hydrothermal ageing (HTA-2) a series of wet runs was performed immediately. As seen in the first section, the three ignition curves were essentially the same. After that, a set of dry experiments was performed. The Arrhenius curves for the wet runs are shown in Figure S22 and those for the dry runs are shown in Figure S23. The data are then summarized in Table S4.

It is seen that the activation energy was essentially constant for all of the methane concentrations, with an average value of approximately 104 kJ/mol. For the dry runs, the activation energies showed the same trend of increasing with an increase in methane concentration, with values similar to those observed previously.

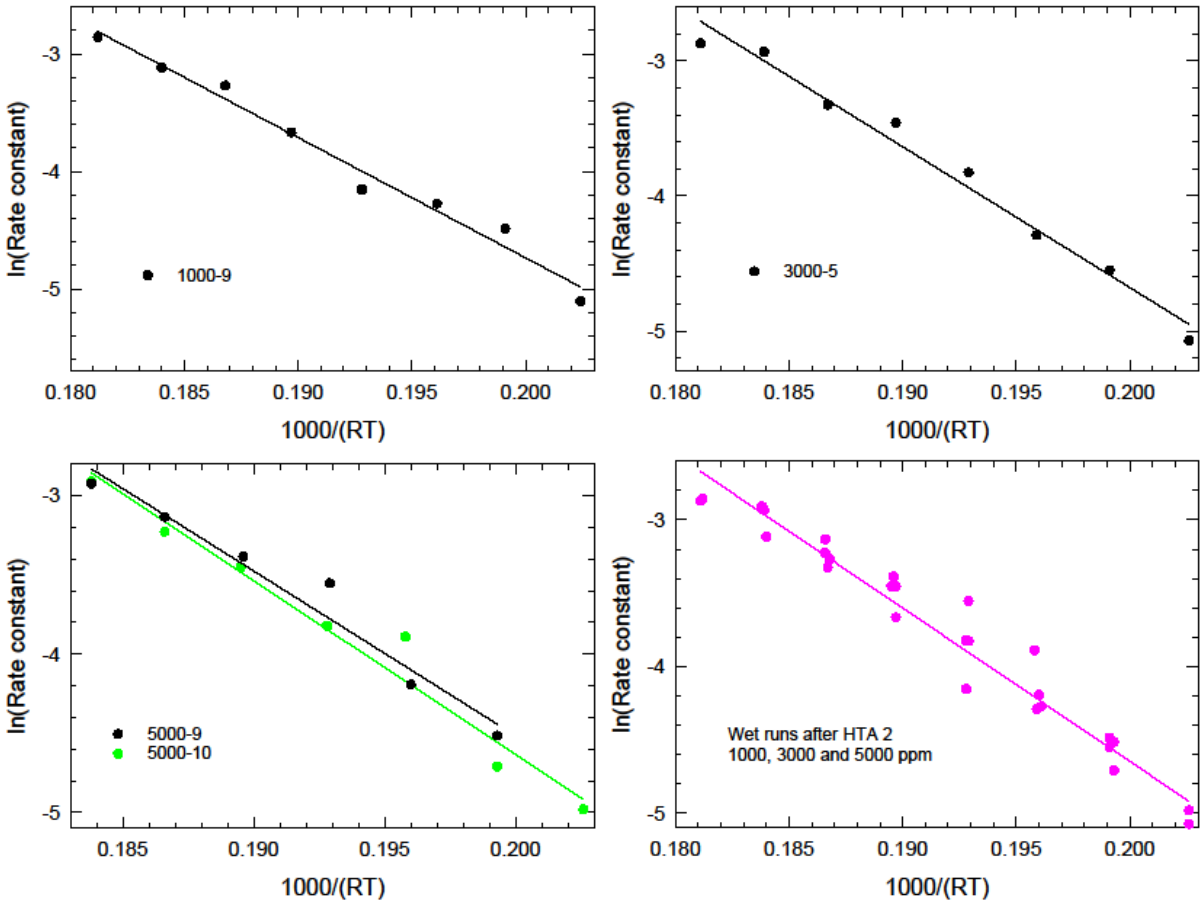

Figure S22 – Arrhenius curves for the wet runs performed immediately after HTA-2.

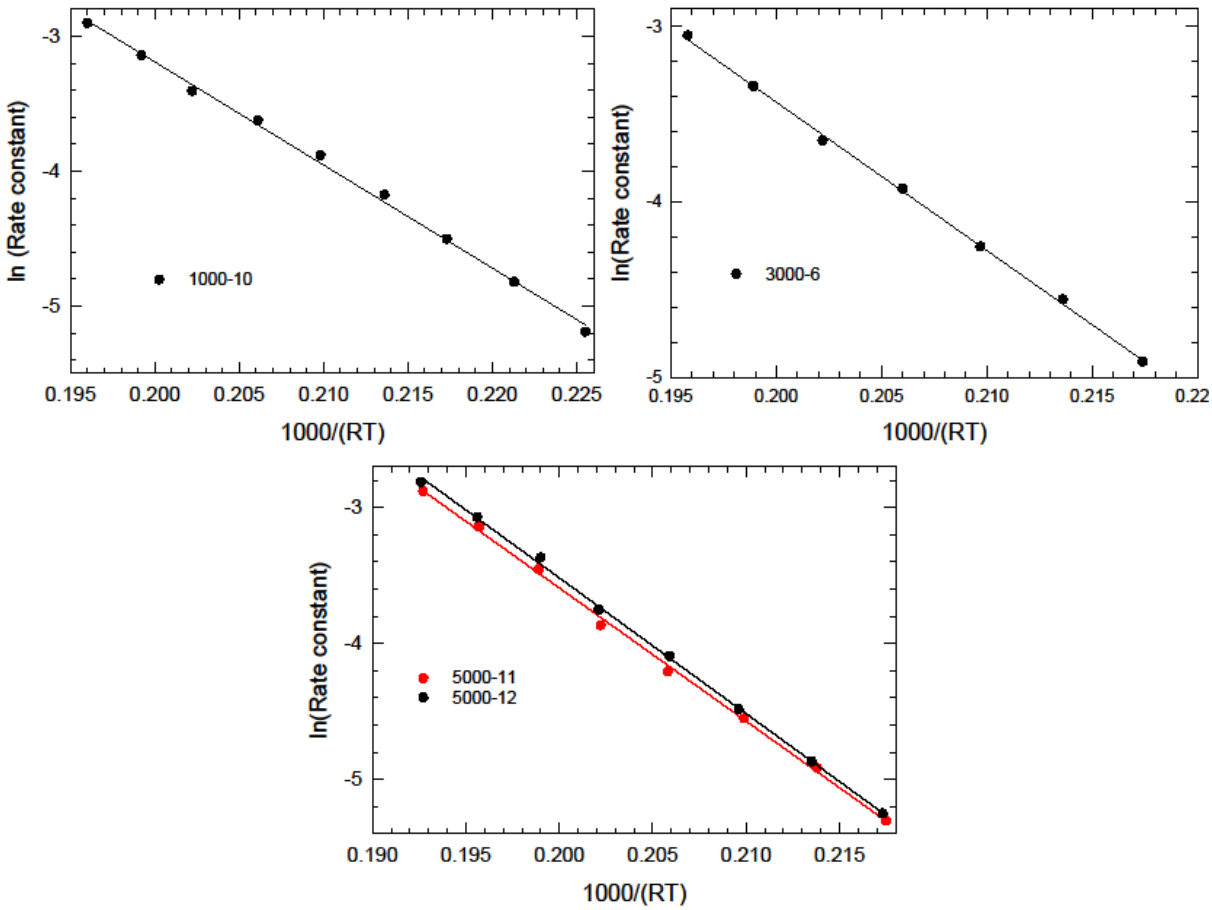

Figure S23 – Arrhenius curves for the dry runs performed after HTA-2.

Table S4 - First order Arrhenius parameters for ignition curves obtained after HTA 2.

Run details	*A*	k_0	*E*
Runs with 2 % added water			
1000-9	15.75	6.92E+06	102.44
3000-5	16.21	1.10E+07	104.44
5000-9	16.27	1.16E+07	103.94
5000-10	17.29	3.23E+07	109.61
combined	16.27	1.16E+07	104.59
Dry runs			
1000-10	12.09	1.78E+05	76.40
3000-6	13.50	7.29E+05	85.65
5000-11	16.00	8.89E+06	97.96
5000-12	16.45	1.39E+07	99.85

First order Arrhenius plots following third hydrothermal ageing

After the third hydrothermal ageing (HTA-3) two wet runs was performed immediately. As seen earlier, the two ignition curves were essentially the same. After that, a set of dry experiments was performed. The Arrhenius curves for the wet runs are shown in Figure 24 and those for the dry runs are shown in Figure 25. The data are then summarized in Table 5.

The activation energies for the wet runs seemed relatively low compared to the results obtained previously. Compared to the results for the dry runs, this is especially true.

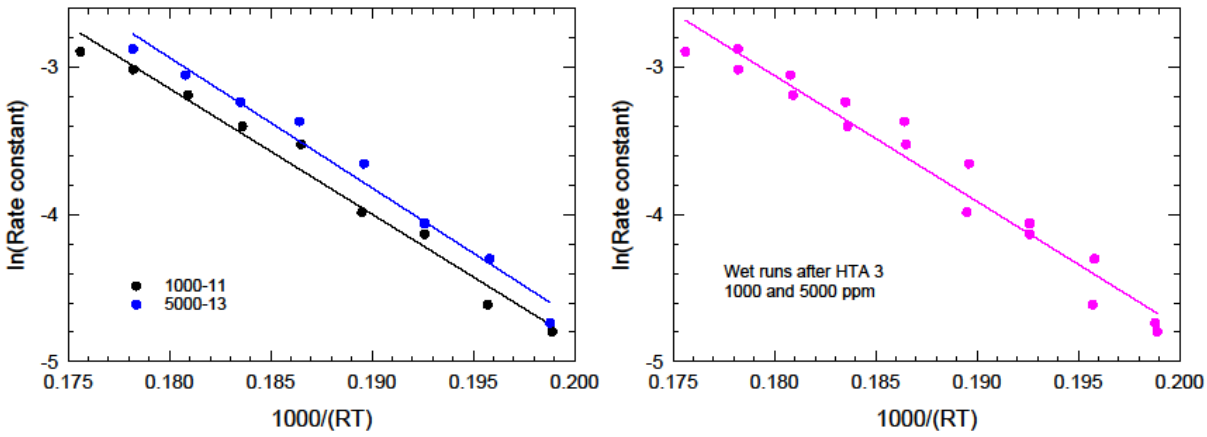

Figure S24 – Arrhenius curves for the wet runs performed immediately after HTA-3.

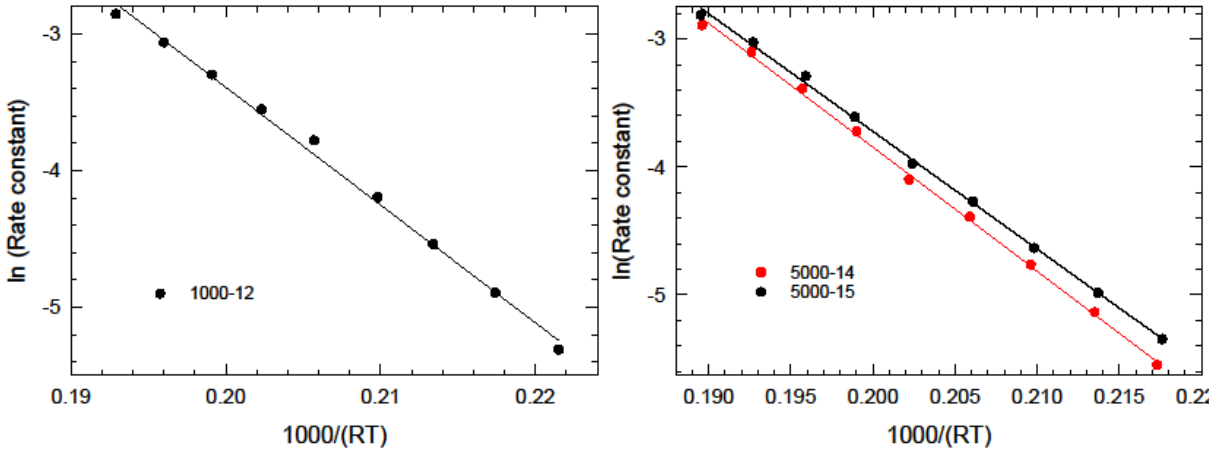

Figure S25 – Arrhenius curves for the dry runs performed immediately after HTA-3.

Table S5 - First order Arrhenius parameters for ignition curves obtained after HTA 3.

Run details	A	k_0	E
Runs with 2 % added water			
1000-11	12.21	2.01E+05	85.34
5000-13	13.01	4.47E+05	88.56
combined	12.33	2.26E+05	85.48
Dry runs			
1000-12	13.86	1.05E+06	86.21
5000-14	15.52	5.50E+06	96.82
5000-15	14.67	2.35E+06	91.98

Rate expression with water inhibition kinetics

The objective of this study was to obtain a rate expression that was suitable for preliminary reactor design for both dry and for wet conditions with 2% water in the feed. Using the data analysis described in the foregoing, such an expression is developed here.

Pd based catalysts are known to be inhibited by water. A classical form rate expression for methane oxidation over Pd has the form:

$$\left(-r_{\mathrm{CH_4}}\right) = \frac{k\,C_{\mathrm{CH_4}}}{1+K\,C_{\mathrm{H_2O}}} = \frac{exp\left(A_0 - \dfrac{E}{R_g T}\right) C_{\mathrm{CH_4}}}{1+K_0\,exp\left(\dfrac{H}{R_g T}\right) C_{\mathrm{H_2O}}} \tag{S7}$$

If the concentration of water is sufficiently large, then the reaction rate may approach the approximate expression:

$$\left(-r_{\mathrm{CH_4}}\right) \approx \frac{k\,C_{\mathrm{CH_4}}}{K\,C_{\mathrm{H_2O}}} \approx \frac{1}{K_0\left(C_{\mathrm{H_2O}}\right)_0} exp\left(A_0 - \frac{(E+H)}{R_g T}\right) C_{\mathrm{CH_4}} \tag{S8}$$

This approximation would be valid for a given water concentration in the feed.

For the case of dry feed, the amount of water can be related to the methane concentration. In terms of fractional conversion and volumetric flow rate, we write:

$$\left(-r_{CH_4}\right) = \frac{k\left(F_{CH_4}\right)_0\left(1-X_{CH_4}\right)}{Q\left(1+K\frac{2}{Q}\left(F_{CH_4}\right)_0 X_A\right)} = \frac{k\left(F_{CH_4}\right)_0\left(1-X_{CH_4}\right)}{\left(Q+2K\left(F_{CH_4}\right)_0 X_A\right)} \quad \text{(S9)}$$

Substitute into the PFR mole balance:

$$\frac{d\,X_{CH_4}}{dW} = \frac{k\left(1-X_{CH_4}\right)}{\left(Q+2K\left(F_{CH_4}\right)_0 X_{CH_4}\right)} \quad \text{(S10)}$$

The equation can be integrated:

$$kW = \int_0^{X_{CH4}} \frac{\left(Q+2K\left(F_{CH_4}\right)_0 X_{CH_4}\right)}{\left(1-X_{CH_4}\right)} d\,X_{CH_4} \quad \text{(S11)}$$

Solving gives a non-linear algebraic equation:

$$kW+\left(Q+2K\left(F_{CH_4}\right)_0\right)ln\left(1-X_{CH_4}\right)+2K\left(F_{CH_4}\right)_0 X_{CH_4} = 0 \quad \text{(S12)}$$

Optimization can be used to find the best values of the kinetic parameters.

Note: For the general case which includes wet feed, the equation is written:

$$\frac{d\,X_{CH_4}}{dW} = \frac{k\left(1-X_{CH_4}\right)}{\left(Q+K\left[\left(F_{H_2O}\right)_0+2\left(F_{CH_4}\right)_0 X_{CH_4}\right]\right)} \quad \text{(S13)}$$

An optimizer was built using Matlab. Two optimization strategies were used, a genetic algorithm and one based on the gradient method. Both tools gave essentially the same results. Only the conversion data between 15 and 85 % were used.

Recall that the rate parameters are expressed as follows:

$$k = exp\left\{A_0 - E\left(\frac{1000}{R_g T}\right)\right\} \qquad K = K_0\, exp\left(H\left(\frac{1000}{R_g T}\right)\right)$$

In the first instance, the seven dry experiments on the fresh catalyst were used. The optimal parameters were found to be:

$$k = exp\left\{13.76-80.80\left(\frac{1000}{R_g T}\right)\right\} \qquad K = 0.0823\, exp\left(21.29\left(\frac{1000}{R_g T}\right)\right)$$

A comparison of the experimental ignition curves and the model predictions for each inlet concentration of methane is shown in Figure S26. The agreement is satisfactory, especially in the conversion region above 20%.

Note: the optimization was also run when the entire conversion range was included. It was observed that in this case the agreement at low conversion (<10%) and high conversion (>90%) was excellent, however the agreement in the range 20-80% was not satisfactory. This result occurs because of the large number of data points in these two regions which artificially weights the result. This phenomenon is exacerbated because we used relative rather than absolute errors to compute the objective function.

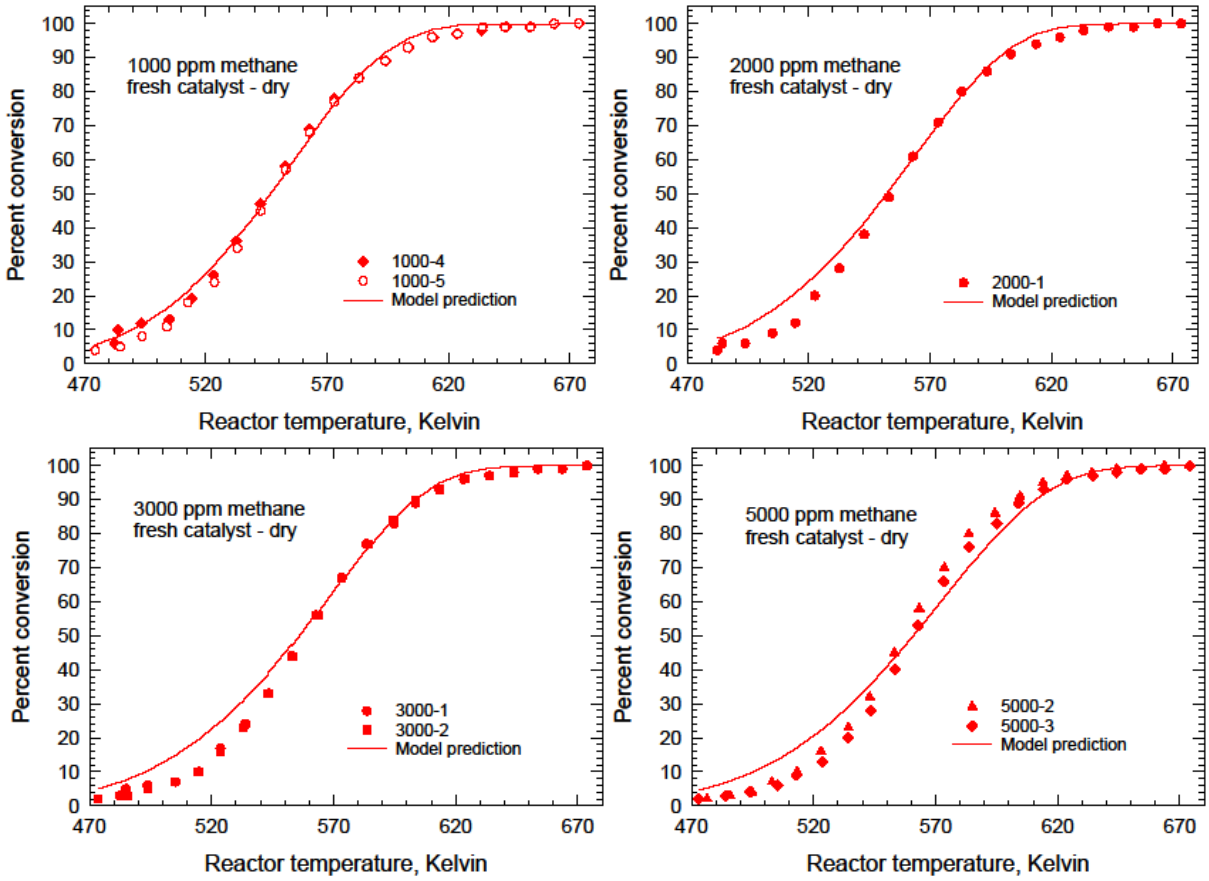

Figure S26 – Comparison of experimental values to model predictions, generalized model. Dry runs on the fresh catalyst. Catalyst 1.

The optimization was also performed for the dry runs obtained after HTA-1 (before the six week break), HTA-2 and HTA-3. As before, only the data between 15 and 85% conversion were used. Five optimizations were performed in each case. In the first one, all four parameters were allowed to vary. Then, the parameters were fixed successively to those obtained in the case of the fresh catalyst. That is, first H was fixed, then H and $K0$, then H, $K0$ and E, and finally H and E. The parameters are summarized in Table 6.

Graphs of the agreements are presented after the table in summary form. One immediate observation is that the value of H can be changed over a quite wide range without affecting the results very significantly.

Table S6 – Parameter values obtained for the optimization of the dry runs are each HTA. Parameters in bold red font were fixed during the optimization.

Series	A	E	K_0	H
Fresh	13.76	80.80	0.0823	21.29
After HTA-1				
Model (a)	17.4982	99.18	0.39726	16.40
Model (b)	17.6842	99.94	0.1536	**21.29**
Model (c)	16.0138	92.94	**0.0823**	**21.29**
Model (d)	13.4547	**80.80**	**0.0823**	**21.29**
Model (e)	13.4698	**80.80**	0.08727	**21.29**
After HTA-2				
Model (a)	17.1851	99.13	0.01	36.7657
Model (b)	18.4793	105.43	0.2356	**21.29**
Model (c)	15.6002	93.30	**0.0823**	**21.29**
Model (d)	13.0276	**80.80**	**0.0823**	**21.29**
Model (e)	13.103	**80.80**	0.10758	**21.29**
After HTA-3				
Model (a)	16.79	99.46	0.0312	29.16
Model (b)	18.3346	106.88	0.1684	**21.29**
Model (c)	12.1205	80.23	**0.0823**	**21.29**
Model (d)	12.2194	**80.80**	**0.0823**	**21.29**
Model (e)	12.823	**80.80**	0.0840	**21.29**
Model (f)	**12.823**	**80.80**	**0.0823**	**21.29**

Figure S27 shows the model agreement for the experiments performed after the first hydrothermal ageing for the five sets of parameter values. It is noticeable that the five model parameter sets all give fairly good agreement. When all of the parameters are allowed to vary, we see that H assumes a fairly low value. However, when H is fixed to the value obtained for the fresh catalyst, and then when both H and K_0 are fixed, the resulting predictions are essentially indistinguishable from each other (that is, Models a, b and c). When both E and H are fixed, the resulting models show a minor difference. This again illustrates that there are a number of sets of parameters that will give essentially similar results.

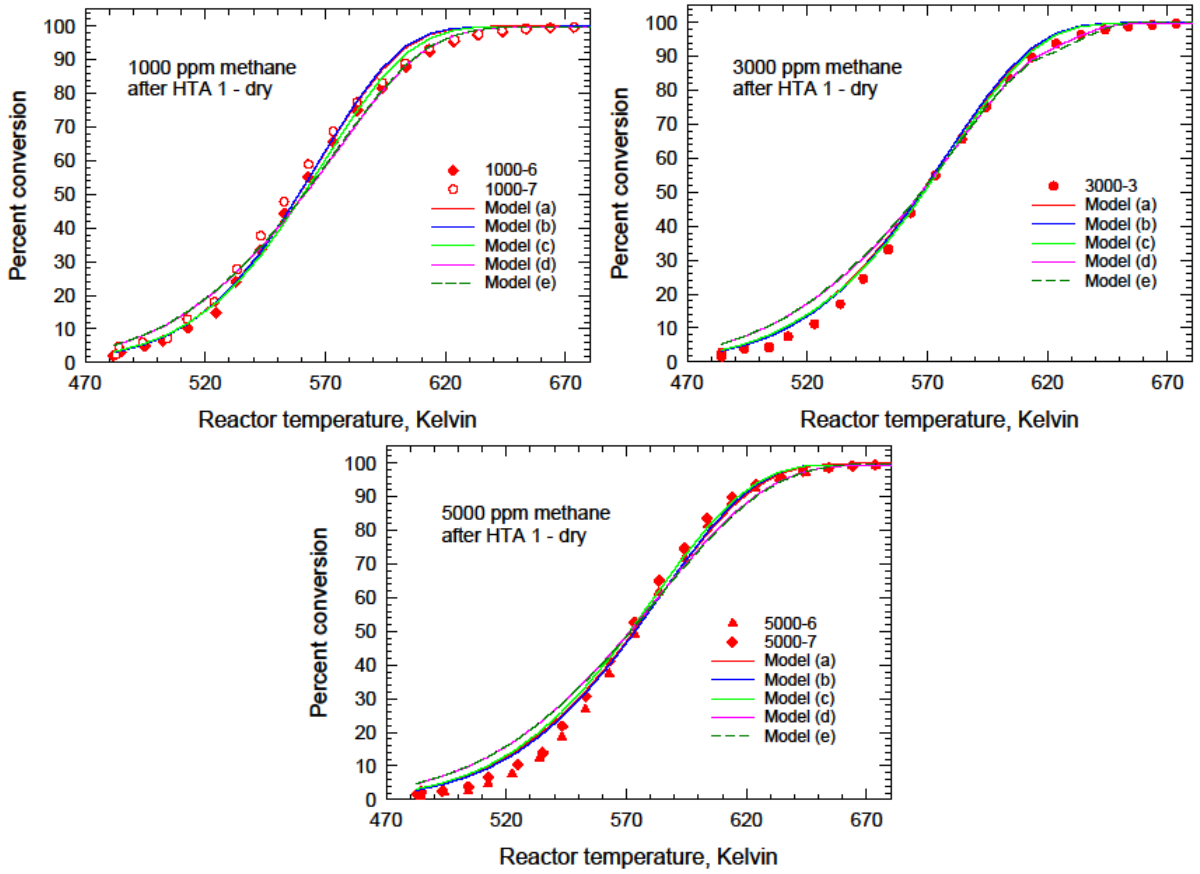

Figure S27 – Plots of the model agreement for the dry runs performed after HTA 1. Models (a), (b) and (c) are virtually indistinguishable, as are models (d) and (e). All of the models give acceptable predictions. Catalyst 1.

Figure S28 shows the model agreement for the experiments performed after the second hydrothermal ageing for the five sets of parameter values. Just as observed for the results from the first HTA, the five model parameter sets all give fairly good agreement. When all of the parameters are allowed to vary, we see that H assumes a fairly high value. However, when H is fixed to the value obtained for the fresh catalyst, and then when both H and K_0 are fixed, the resulting predictions are essentially indistinguishable from each other (that is, Models a, b and c), although Model (c) is slightly different from (a) and (b) for 1000 ppm methane. Models (d) and (e) are again similar.

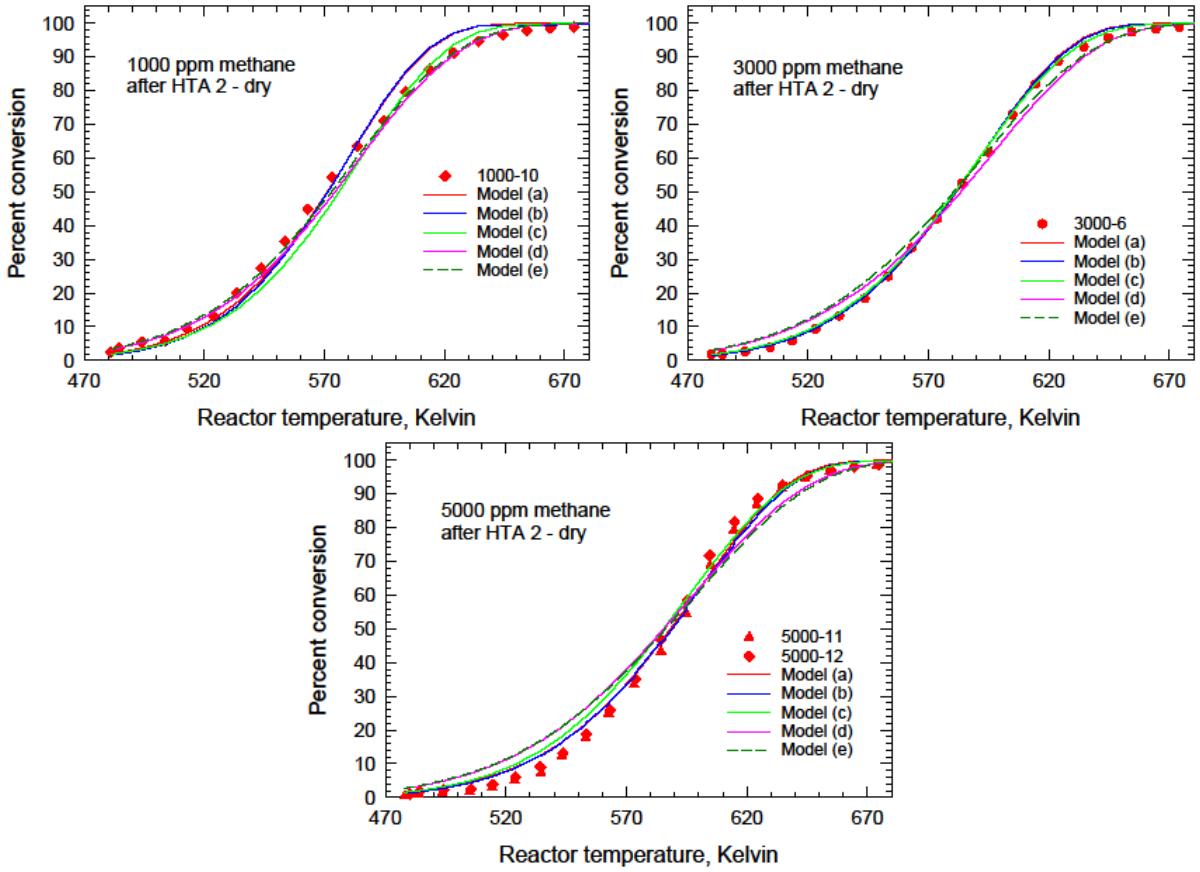

Figure S28 – Plots of the model agreement for the dry runs performed after HTA 2. Models (a) and (b) are virtually indistinguishable, as are models (d) and (e). For model (c) it lies between these two pairs. All of the models give acceptable predictions. Catalyst 1.

Figure S29 shows the model agreement for the experiments performed after the third hydrothermal ageing for the five sets of parameter values. In this case, the Model (a) value for H was closest to the one observed for the fresh catalyst.

Models (a) and (b) are the same. Models (c) and (d) are the same. It is strange that Models (c) and (d) look so anomalous, because in both cases the values of E, H and K_0 are similar to the ones in Model (e) which fits the data well. Therefore, a final Model, called (f) is shown, in which all parameter values in the rate model were fixed as shown in Table S6. This Model shows good agreement, and is essentially the same as Model (e), with the most deviation being observed at the lower conversions.

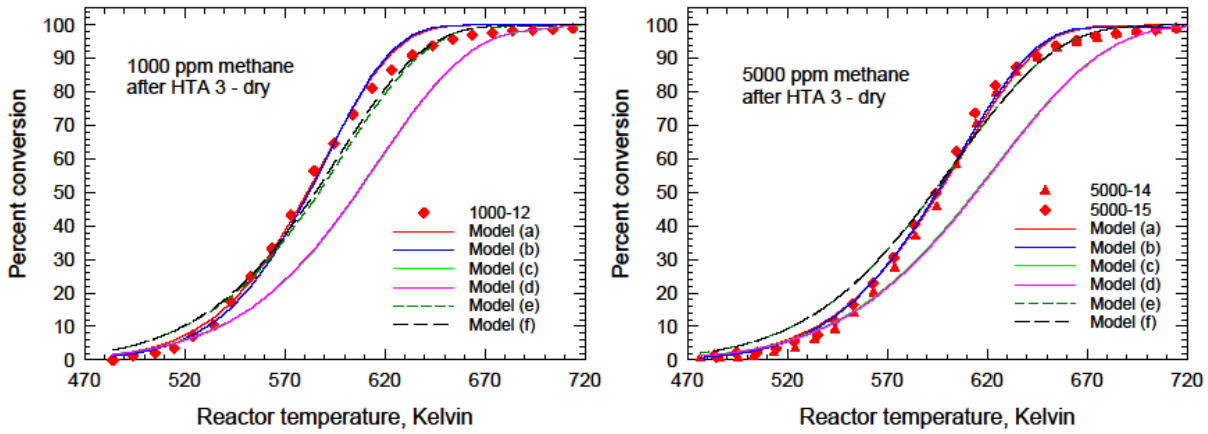

Figure S29 – Plots of the model agreement for the dry runs performed after HTA 3. Models (a) and (b) are virtually indistinguishable, as are models (c) and (d). Models (e) and (f) are also essentially the same. Catalyst 1.

We can draw some overall conclusions for these dry runs. The first is that are a range of parameter values that will give an agreeable fit, so the values shown should not necessarily be considered as absolute. In particular, the model is fairly insensitive to the value of H, provided the other parameters are allowed to adjust. Finally, it is interesting to observe that there is a set of common values for E, K_0 and H that gives an acceptable fit for the four levels of catalyst activity, with only the value of A being adjusted to reflect the deactivation.

Kinetic model for the case with 2% water in the feed

As shown earlier, the ignition curves obtained when 2% water was added to the feed were essentially independent of the inlet methane concentration. Therefore, a first order rate model is a close approximation for the result, because the water inhibition term in

the denominator dominates the result. In the first instance, the kinetic parameters obtained using the Arrhenius analysis shown earlier were used to generate the ignition curves. The result is shown in Figure S30, denoted Model (a). As a second step, the first order rate parameters were optimized using all of the data, including those at low and high concentration. However, note that for this optimization absolute errors were used, to reduce the influence of the low and high conversion data. The resulting parameters were very similar, and the predicted ignition curve is also shown in Figure S25 as Model (b). The parameters for the two models are given in Table S7. As seen from both the graphs and the table of data the results are very close in both cases.

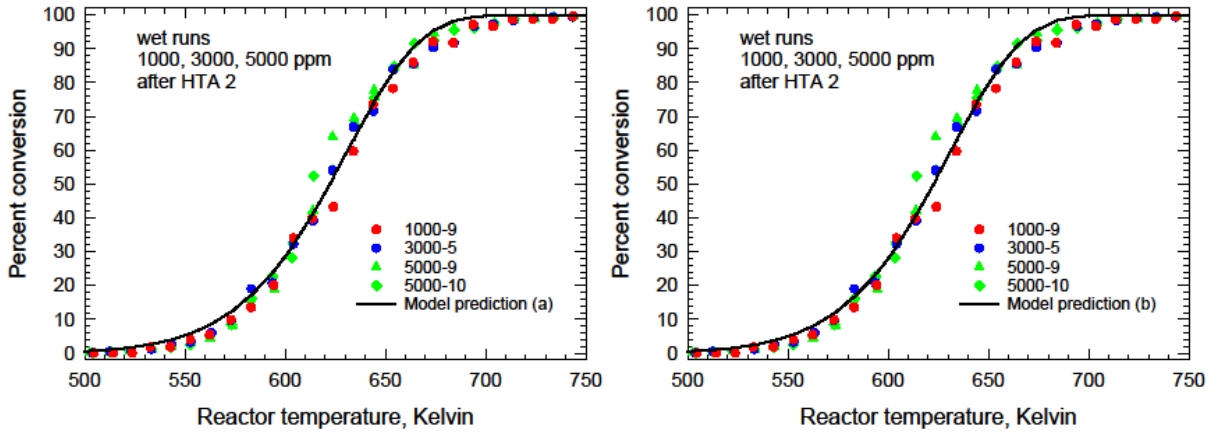

Figure S30 – Predicted ignition curves for the wet runs obtained after HTA 2 for the two sets of model parameters. See Table 7. Catalyst 1.

Table S7 – Parameters for the pseudo-first order rate expression used for the runs with 2% water added obtained after HTA 2.

Model	*A*	*E*
Model (a)	16.27	104.59
Model (b)	16.58	106.26

A similar analysis was performed on the wet ignition curves obtained after HTA 3 and the results are shown in Figure S31. In the first instance, the values obtained from the Arrhenius analysis performed earlier were used, denoted Model (a). Because the apparent activation energy obtained from the Arrhenius plot appeared to much lower than expected, the data were optimized again by fixing the apparent activation energy to 104.59 kJ/mol, the value obtained for the wet runs after HTA 2. The optimization was done using absolute error to calculate the objective function, and was performed using

both the data between 15 and 85% conversion and the entire data set. The result was the same in both cases. This result is also shown in Figure S31 as Model (b). Finally, the data were re-optimized using the entire data set allowing both parameters to vary. This result is denoted Model (c). The parameters obtained in each case are summarized in Table S8.

In conclusion, we can say that there is a common model for the wet runs that will fit both levels of catalyst activity, that is, with a common value for the apparent activation energy and only the pre-exponential factor changing to reflect the level of catalyst activity.

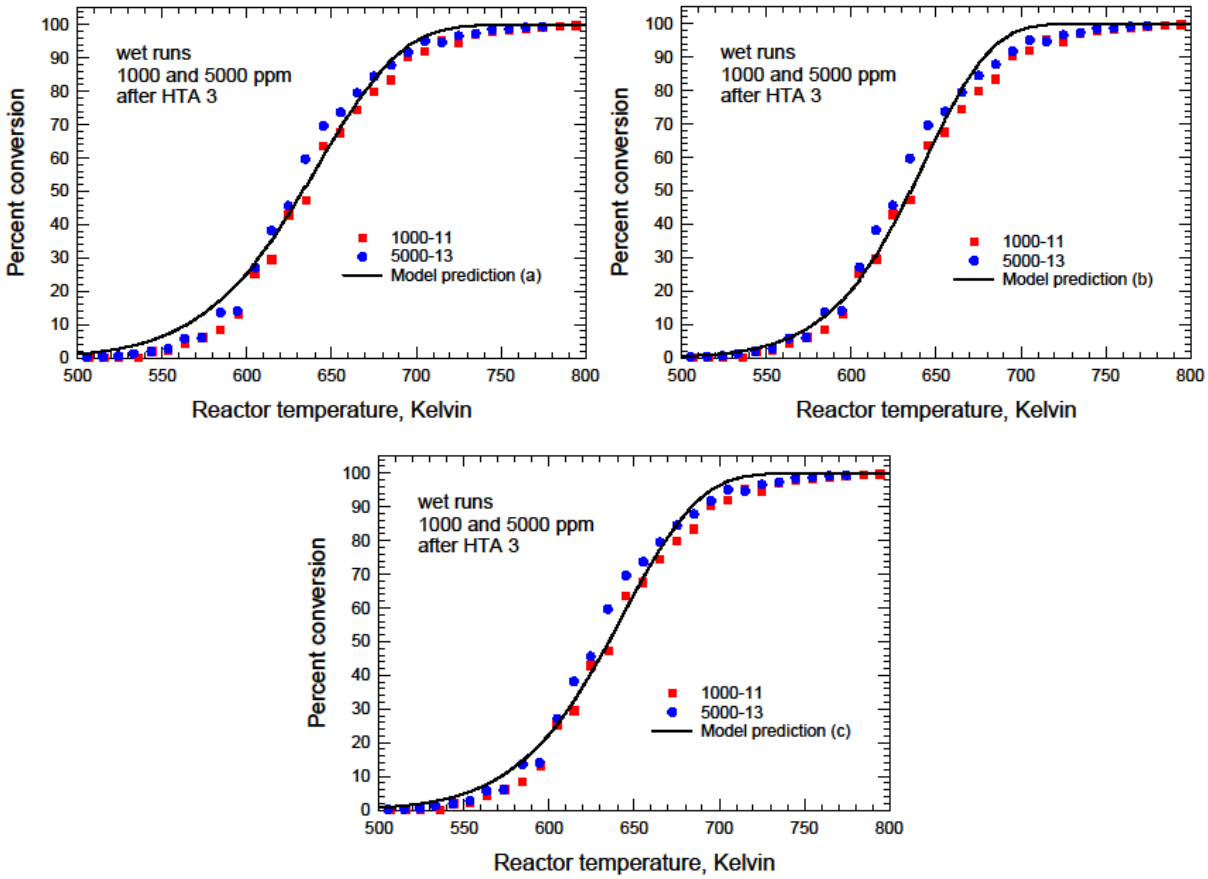

Figure S31 - Predicted ignition curves for the wet runs obtained after HTA 3 for the three sets of model parameters. See Table S8. Catalyst 1.

Table S8 – Parameters for the pseudo-first order rate expression used for the runs with 2% water added obtained after HTA 3 for the three models. Catalyst 1.

Model	*A*	*E*
Model (a)	12.33	85.48
Model (b)	15.90	104.59
Model (c)	13.88	93.89

Conclusion

The final conclusion is that we can use a common reaction rate model for the dry runs, adjusting the value for the pre-exponential factor to reflect the catalyst activity. Similarly, for the runs with 2 % added water, we can use a first order reaction rate model with a common apparent activation energy, and again adjusting the pre-exponential factor to reflect the catalyst activity.

Results for the home-made catalysts.

Figures (S32 to S36) show the Arrhenius plots obtained for Catalysts 2 to 6. We show the results for a regression analysis for each concentration separately, and then the curve for all of the data at all concentrations.

The first order rate parameters were determined by regression analysis for each methane concentration separately, and for all of the data at all concentrations. The parameters are shown in Table S9. The complex model with water inhibition, represented by the following equation, was then optimized using the Matlab program. The resulting parameters are given in Table S10.

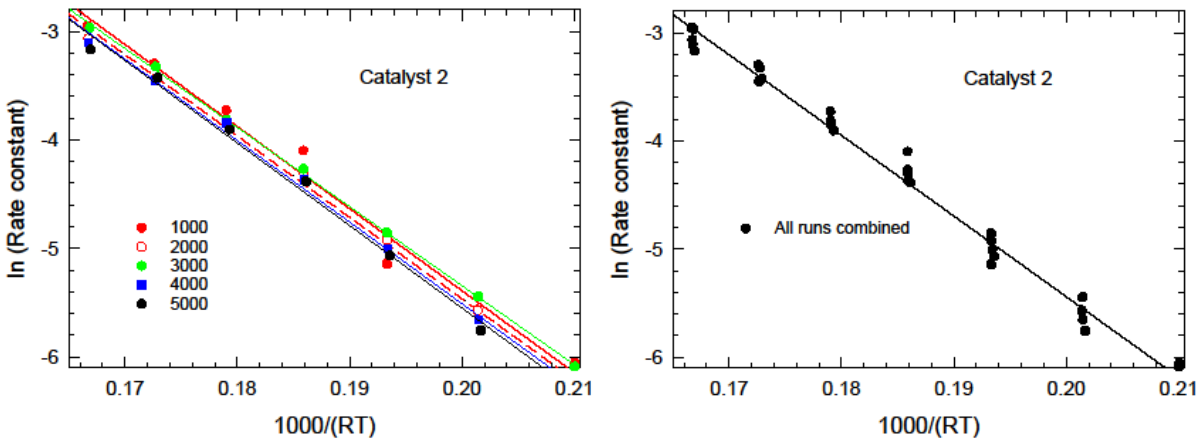

Figure S32 - Arrhenius plots for the first order reaction analysis for Catalyst 2

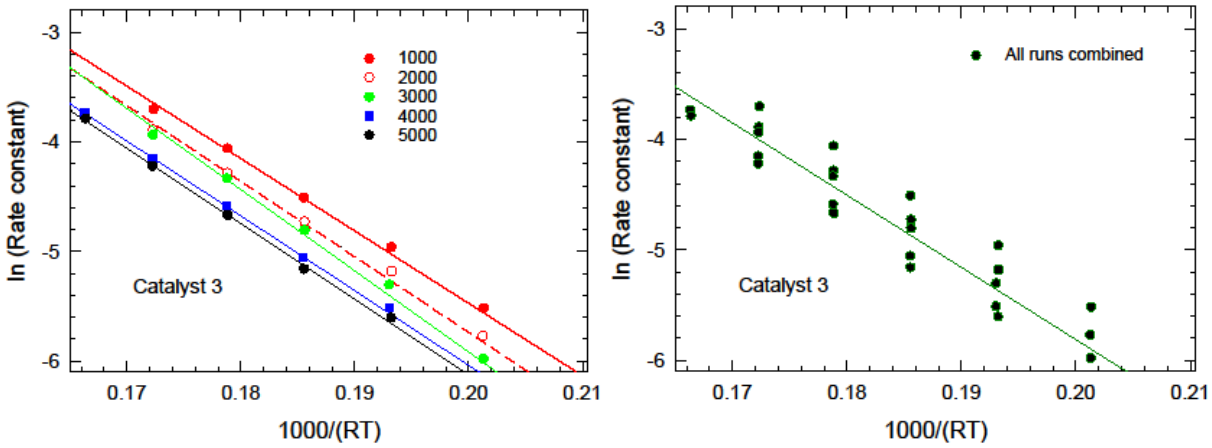

Figure S33 -Arrhenius plots for the first order reaction analysis for Catalyst 3

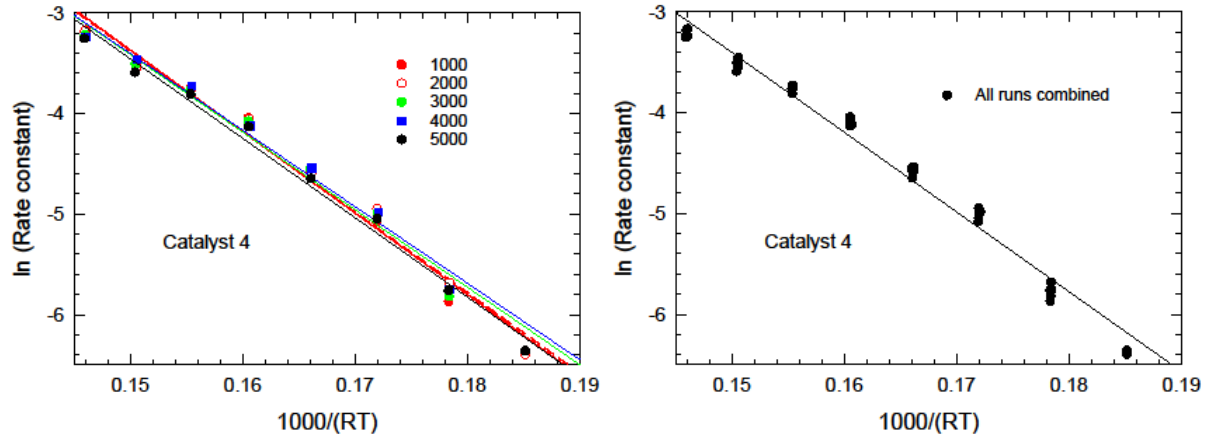

Figure S34 -Arrhenius plots for the pseudo first order reaction analysis for Catalyst 4

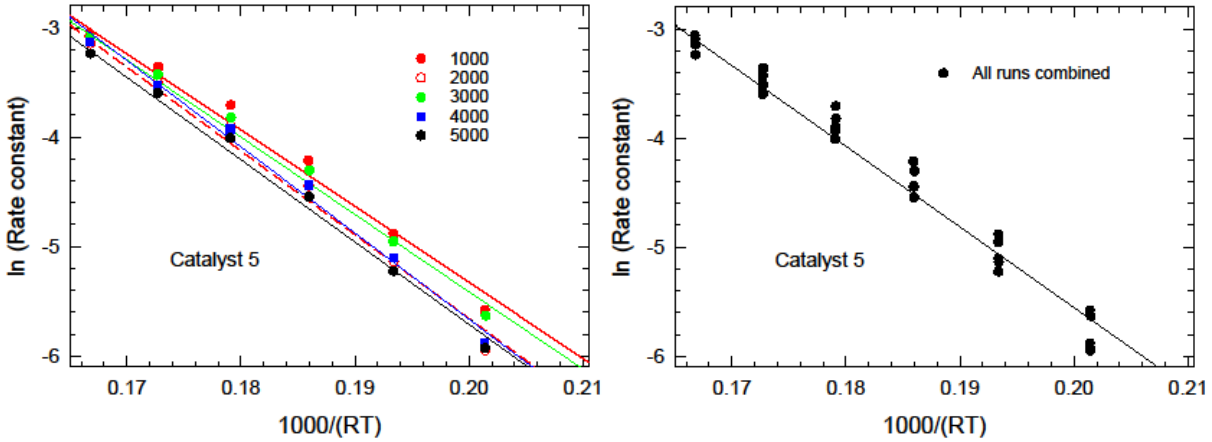

Figure S35 - Arrhenius plots for the first order reaction analysis for Catalyst 5

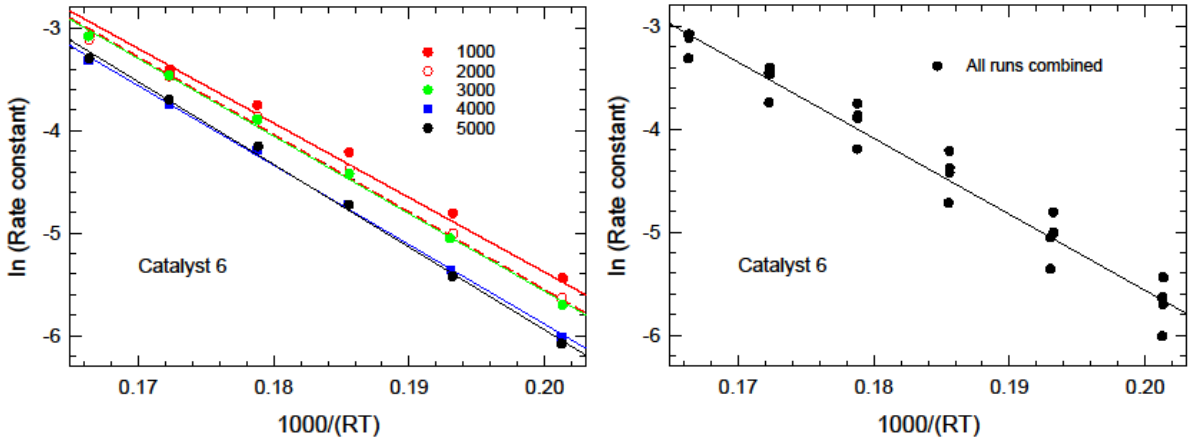

Figure S36 - Arrhenius plots for the first order reaction analysis for Catalyst 6

Table S9 - Summary of pseudo-first order fitting for Catalysts 2 to 6. The activation energy has units of kJ/mol.

ppm	1000	2000	3000	4000	5000	all
Catalyst 2						
A	9.74	9.54	9.24	9.53	9.67	9.48
E	75.6	75.0	72.9	75.2	76.1	74.6
Catalyst 3						
A	7.74	8.07	8.91	7.62	7.65	7.26
E	66.1	69.1	74.1	68.3	68.9	65.3
Catalyst 4						
A	8.79	8.63	8.16	8.02	8.4	8.46
E	81.1	80.0	77.1	76.1	79.0	79.0
Catalyst 5						
A	8.59	9.65	8.72	10.1	9.34	9.23
E	69.6	76.6	70.6	78.8	75.2	73.9
Catalyst 6						
A	9.16	9.58	9.58	9.62	10.2	9.22
E	72.7	75.7	75.7	77.5	80.7	73.9

Table S10 - Summary of complex model fitting for Catalysts 2 to 6. The activation energy has units of kJ/mol.

Catalyst	*A*	*E*	K_0	*H*
2	10.6	79.9	2.18	1.81
3	10.4	77.1	0.1	29.2
4	8.6	79.3	0.812	1.0×10^{-4}
5	10.1	77.3	5.4	1.3×10^{-4}
6	10.0	75.4	4.1×10^{-3}	45.7

Note that these parameters should not necessarily be considered unique. As was seen for Catalyst 1 with thie same complex rate model for the dry runs at different levels of catalyst activity, there are multiple sets of parameters that can give ignition curves that are virtually indistinguishable with the naked eye, and have very small differences in the values of he objective function. For Catalysts 2 to 6 we have simply let the Matlab optimizer find the best values of the objective function, and have not done any sensitivity analysis on the parameter values. We are simply trying to show the differences between the fits that are possible with this complex model compared to the pseudo first order model.

Figures S37 to S41 compare the model fits for the first order and the complex model for Catalysts 2 to 6 for each of the concentrations.

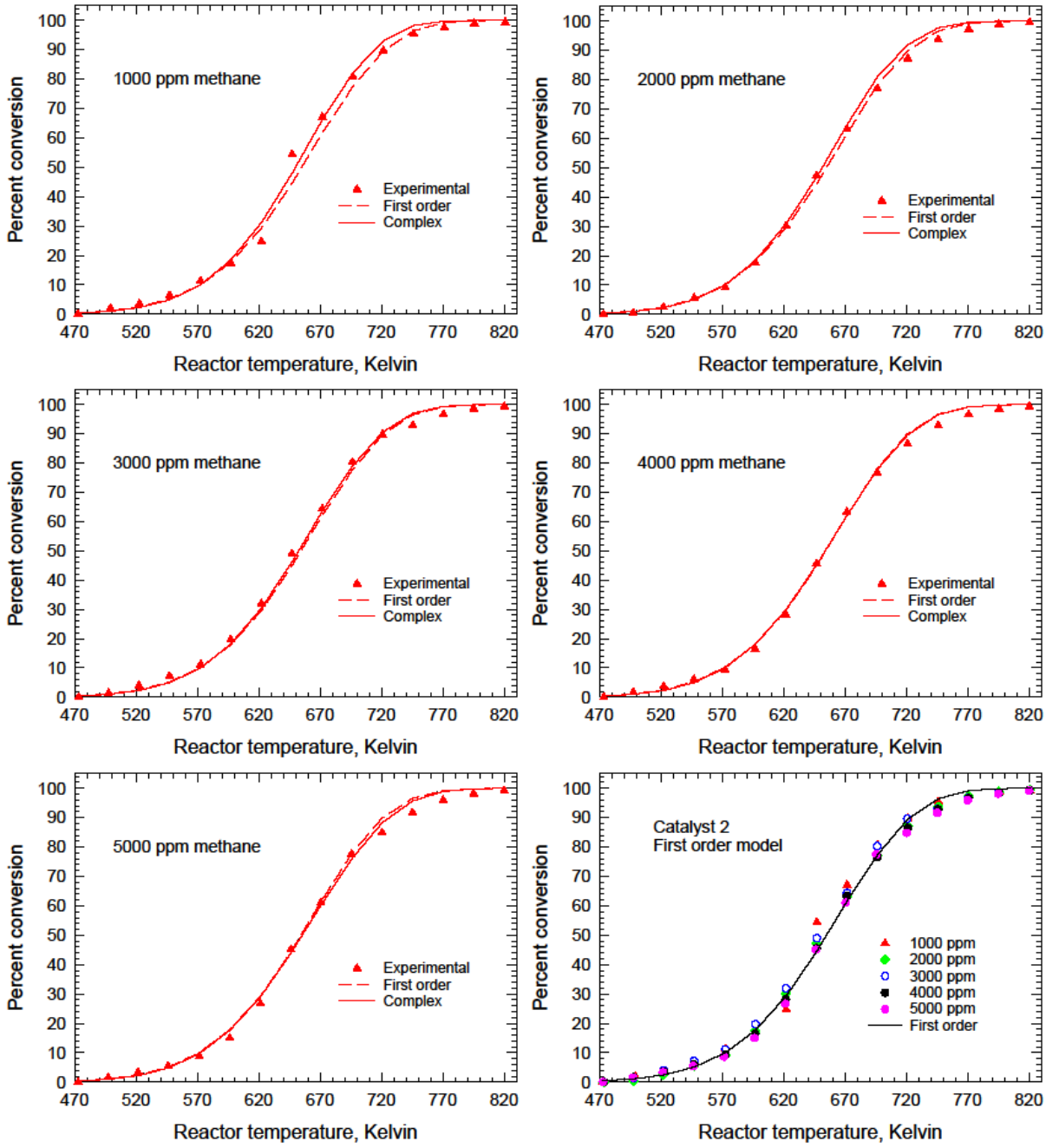

Figure S37 - Comparison of model fits for Catalyst 2 for the first order and complex model. A first order model fits the data reasonably well.

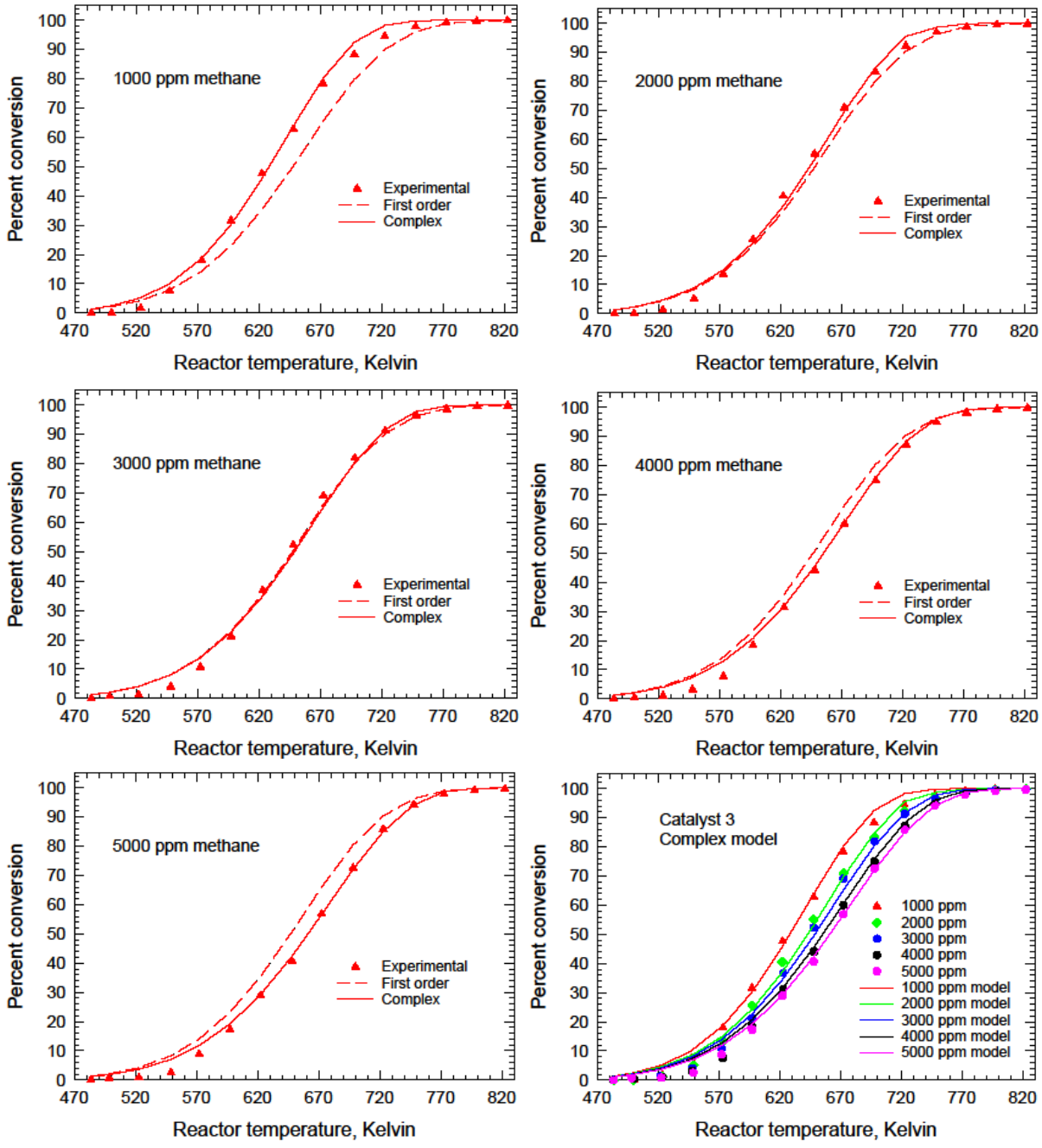

Figure S38 - Comparison of model fits for Catalyst 3 for the first order and complex model. The complex model fits the data reasonably well.

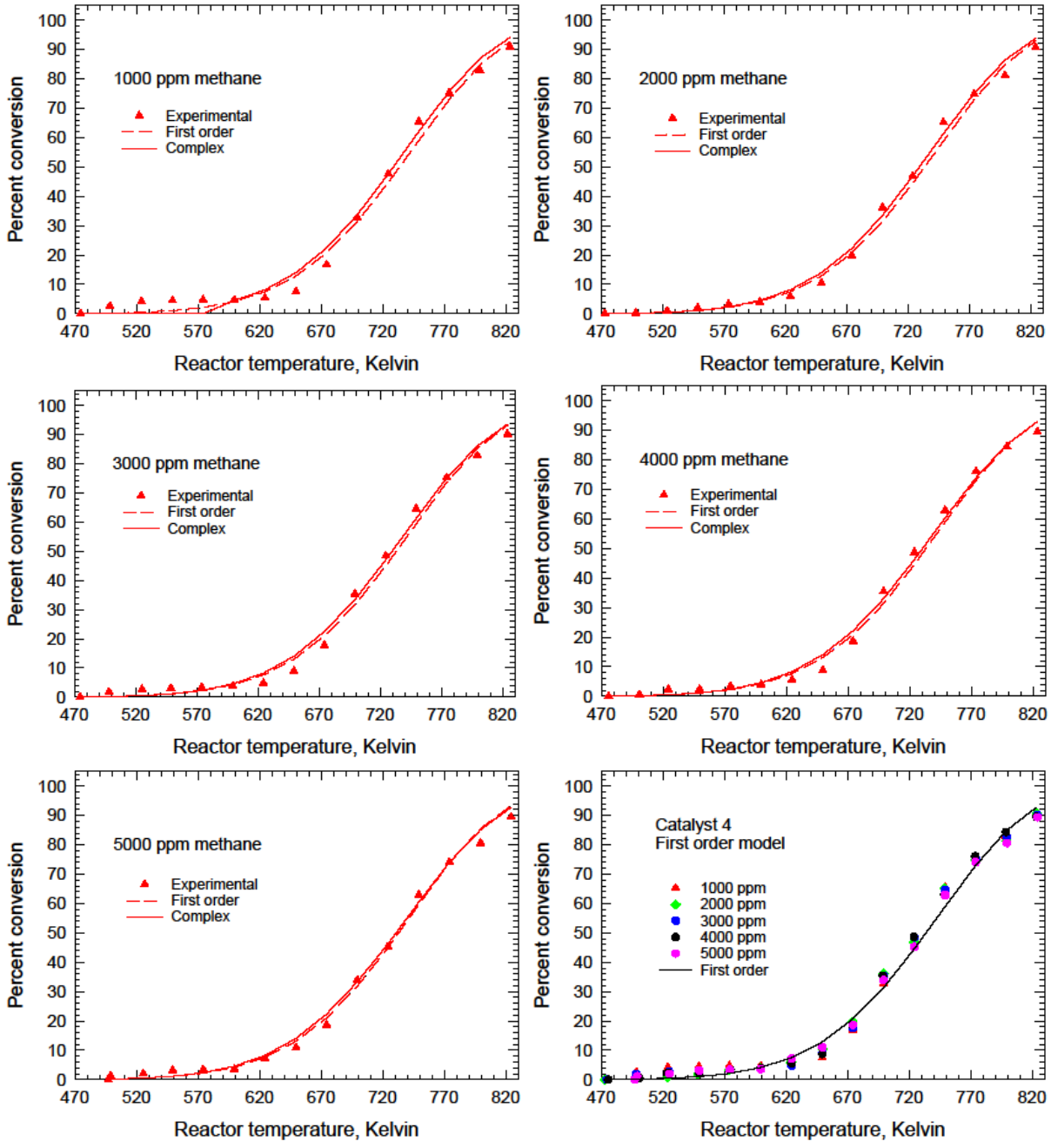

Figure S39 - Comparison of model fits for Catalyst 4 for the first order and complex model. A first order model fits the data reasonably well.

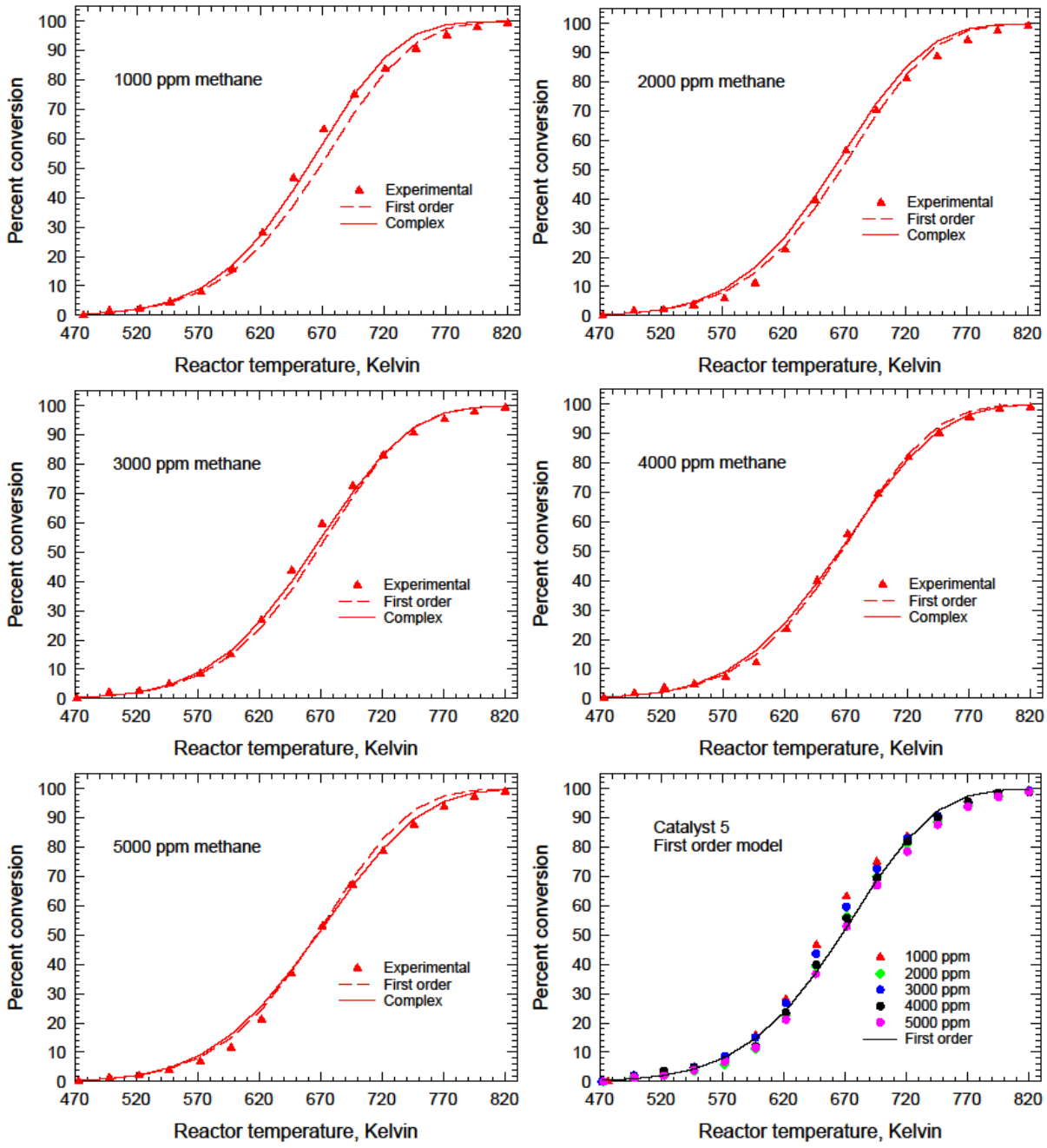

Figure S40 - Comparison of model fits for Catalyst 5 for the first order and complex model. A first order model fits the data reasonably well.

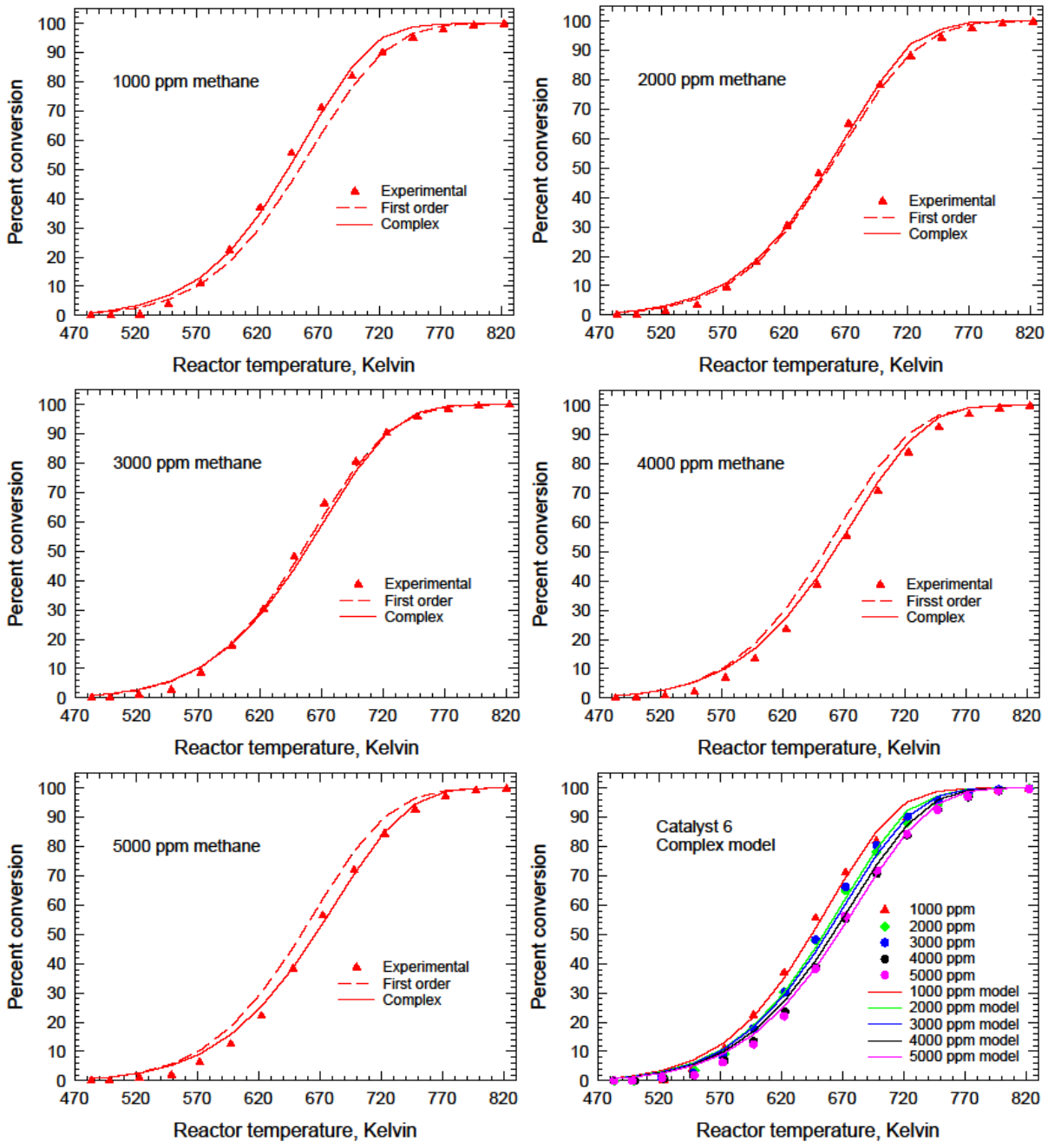

Figure S41 - Comparison of model fits for Catalyst 6 for the first order and complex model. The complex model fits the data reasonably well.

Assumptions of plug flow and absence of heat and mass transfer limitations.

The following sections show calculations that verify the plug flow assumption and demonstrate that the assumption of kinetic control is valid. The calculations are reproduced from earlier publications with minor modifications as stated in the following.

The calculations for Catalyst 2 ($Pd/Co/SnO_2$) and Catalyst 5 ($PdPt/Co/Al_2O_3$) are reprinted from reference [136] with permission from Elsevier, and the calculations for Catalyst 6 ($PdPt/Al_2O_3$) and Catalyst 3 ($PdPt/SnO_2$) are reprinted from reference [121] with permission from Elsevier.

Verification of ideal plug flow conditions

The kinetic modelling technique used in this investigation assumed plug flow. The following example calculations for selected catalysts demonstrate the validity of this assumption.

Catalyst 2- Verification of Plug Flow conditions for Pd-Pt/10Co/SnO_2 catalyst

Amount of catalyst + diluent = 0.34 + 0.25 = 0.59 g
Based on measured density of catalyst + diluent = 0.583 g/mL
Bed volume = 0.59/0.583 = 1.012 mL
Reactor ID = 0.9525 cm (3/8 ″)
Bed length = (1.012 * 4)/(π * 0.9525²) = 1.42 cm

Step 1: Dynamic Viscosity of Air at Atmospheric Pressure and 673.15 K

$\mu = 3.4\times10^{-5}$ Ns/m² (Lyons et al., 2016)

Step 2: Calculation of Superficial Velocity

$u = Q/A_c$

Reactor I.D. = 3/8'' = 0.009525 m

$A_c = (\pi/4)*d_p^2 = 7.1256\times10^{-5}$ m²

$Q_0 = 210$ mL/min $= 3.5\times10^{-6}$ m³/s

$Q = Q_0 * (T/273.15) * (1/1.323) = 3.5\times10^{-6} * (673.15/273.15) * (1/1.323) = 6.52 \times10^{-6}$ m^3/s

$u = 3.04\times10^{-6} / 7.1256\times10^{-5} = 0.0915$ m/s (Dautzenberg, 1989)

Step 3: Calculate Particle Reynolds Number

ϱ of air at 673.15K = 0.5247 kg/m^3

$d_P = 5\times10^{-5}$ m

$^{N}Re_P = (0.0915 * 0.5247 * 5\times10^{-5})/(3.4\times10^{-5}) = 0.0706$ (Dautzenberg, 1989)

Step 4: Calculate the Peclet Number (for gas-phase operations)

L = 0.0142 m

$N_{Pe} = 0.087 * (0.0706)^{0.23} * (0.0142/5\times10^{-5}) = 13.43$ (Dautzenberg, 1989)

Step 5: Calculate the Minimum Peclet Number (for gas-phase operations)

n (order of reaction) = 1

X (conversion) = 0.5 (50%)

$^{N}Pe_{min} = 8 * 1 * \ln(1/(1-0.5)) = 5.5452$ (Dautzenberg, 1989)

Step 6: Calculate minimum L/d_P

$L/d_P > 92 * 13.43^{-0.23} * 1 * \ln(1/(1-0.5)) = 35.09$

In our case, L/dp = 284 (Dautzenberg, 1989)

Hence, the condition is satisfied for plug flow

Catalyst 3 - Verification of Plug Flow conditions for Pd-Pt/SnO_2 catalyst

Amount of catalyst + diluent = 0.34 + 0.25 = 0.59 g
Based on measured density of catalyst + diluent = 0.5017 g/mL
Bed volume = 0.59/0.5017 = 1.176 mL

Reactor ID = 0.9525 cm (3/8 ″)
Bed length = (1.176 * 4)/(π * 0.9525^2) = 1.65 cm

Step 1: Dynamic Viscosity of Air at Atmospheric Pressure and 673.15 K

$\mu = 3.4\times10^{-5}$ Ns/m^2 (Lyons et al., 2016)

Step 2: Calculation of Superficial Velocity

$u = Q/A_c$

Reactor I.D. = 3/8" = 0.009525 m

$A_c = (\pi/4)*d_p^2 = 7.1256\times10^{-5}$ m^2

$Q_0 = 210$ mL/min $= 3.5\times10^{-6}$ m^3/s

$Q = Q_0 * (T/273.15) * (1/2.837) = 3.5\times10^{-6} * (673.15/273.15) * (1/2.837) = 3.04\times10^{-6}$ m^3/s

$u = 3.04\times10^{-6} / 7.1256\times10^{-5} = 0.04266$ m/s (Dautzenberg, 1989)

Step 3: Calculate Particle Reynolds Number

ρ of air at 673.15K = 0.5247 kg/m^3

$d_p = 5\times10^{-5}$ m

$^{N}Re_P = (0.04266 * 0.5247 * 5\times10^{-5})/(3.4\times10^{-5}) = 0.03292$ (Dautzenberg, 1989)

Step 4: Calculate the Peclet Number (for gas-phase operations)

L = 0.0165 m

$N_{Pe} = 0.087 * (0.03292)^{0.23} * (0.0165/5\times10^{-5}) = 13.09$ (Dautzenberg, 1989)

Step 5: Calculate the Minimum Peclet Number (for gas-phase operations)

n (order of reaction) = 1

X (conversion) = 0.5 (50%)

$^{N}Pe_{min} = 8 * 1 * \ln(1/(1-0.5)) = 5.5452$ (Dautzenberg, 1989)

Step 6: Calculate minimum L/d_p

$L/d_p > 92 * 13.09^{-0.23} * 1 * \ln(1/(1-0.5)) = 35.30$

In our case, L/dp = 330 (Dautzenberg, 1989)

Hence, the condition is satisfied for plug flow

Catalyst 5 - Verification of Plug Flow conditions for Pd-Pt/10Co/γ-Al_2O_3 catalyst

Amount of catalyst + diluent = 0.34 + 0.25 = 0.59 g
Based on measured density of catalyst + diluent = 0.4223 g/mL
Bed volume = 0.59/0.4223 = 1.397 mL
Reactor ID = 0.9525 cm (3/8 ″)
Bed length = (1.397 * 4)/(π * 0.9525^2) = 1.96 cm

Step 1: Dynamic Viscosity of Air at Atmospheric Pressure and 673.15 K

$\mu = 3.4\times10^{-5}$ Ns/m^2 (Lyons et al., 2016)

Step 2: Calculation of Superficial Velocity

$u = Q/A_c$

Reactor I.D. = 3/8" = 0.009525 m

$A_c = (\pi/4)*d_p^2 = 7.1256 \times10^{-5}$ m^2

$Q_0 = 210$ mL/min $= 3.5\times10^{-6}$ m^3/s

$Q = Q_0 * (T/273.15) * (1/1.17) = 3.5\times10^{-6} * (673.15/273.15) * (1/1.17) = 7.39\times10^{-6}$ m^3/s

$u = 7.39\times10^{-6} / 7.1256\times10^{-5} = 0.1038$ m/s (Dautzenberg, 1989)

Step 3: Calculate Particle Reynolds Number

ϱ of air at 673.15K = 0.5247 kg/m^3

$d_p = 5\times10^{-5}$ m

$^{N}Re_P = (0.1038 * 0.5247 * 5\times10^{-5})/(3.4\times10^{-5}) = 0.08001$ (Dautzenberg, 1989)

Step 4: Calculate the Peclet Number (for gas-phase operations)

L = 0.0196 m

$N_{Pe} = 0.087 * (0.08001)^{0.23} * (0.0196/5\times10^{-5}) = 19.08$ (*Dautzenberg, 1989)

Step 5: Calculate the Minimum Peclet Number (for gas-phase operations)

n (order of reaction) = 1

X (conversion) = 0.5 (50%)

$^{N}Pe_{min} = 8 * 1 * \ln(1/(1-0.5)) = 5.5452$ (Dautzenberg, 1989)

Step 6: Calculate minimum L/d_p

$L/d_p > 92 * 19.08^{-0.23} * 1 * \ln(1/(1-0.5)) = 32.37$

In our case, L/dp = 392 (Dautzenberg, 1989)

Hence, the condition is satisfied for plug flow

Catalyst 6 - Verification of Plug Flow conditions for Pd-Pt/γ-Al_2O_3 catalyst

Amount of catalyst + diluent = 0.34 + 0.25 = 0.59 g
Based on measured density of catalyst + diluent = 0.6115 g/mL
Bed volume = 0.59/0.6115 = 0.9648 mL
Reactor ID = 0.9525 cm (3/8 ″)
Bed length = (0.9648 * 4)/(π * 0.9525^2) = 1.35 cm

Step 1: Dynamic Viscosity of Air at Atmospheric Pressure and 673.15 K

$\mu = 3.4\times10^{-5}$ Ns/m^2 (Lyons et al., 2016)

Step 2: Calculation of Superficial Velocity

$u = Q/A_c$

Reactor I.D. = 3/8" = 0.009525 m

$A_c = (\pi/4)*d_p^2 = 7.1256\times10^{-5}$ m^2

$Q_0 = 210$ mL/min $= 3.5\times10^{-6}$ m^3/s

$Q = Q_0 * (T/273.15) * (1/2.837) = 3.5\times10^{-6} * (673.15/273.15) * (1/2.837) = 3.04\times10^{-6}$ m^3/s

$u = 3.04\times10^{-6} / 7.1256\times10^{-5} = 0.04266$ m/s (Dautzenberg, 1989)

Step 3: Calculate Particle Reynolds Number

ρ of air at 673.15K = 0.5247 kg/m^3

$d_P = 5\times10^{-5}$ m

$^{N}Re_P = (0.04266 * 0.5247 * 5\times10^{-5})/(3.4\times10^{-5}) = 0.03292$ (Dautzenberg, 1989)

Step 4: Calculate the Peclet Number (for gas-phase operations)

L = 0.0135 m

N_{Pe} = 0.087 * $(0.03292)^{0.23}$ * $(0.0135/5\times10^{-5})$ = 10.71 (Dautzenberg, 1989)

Step 5: Calculate the Minimum Peclet Number (for gas-phase operations)

n (order of reaction) = 1

X (conversion) = 0.5 (50%)

$^{N}Pe_{min}$ = 8 * 1 * ln(1/(1-0.5)) = 5.5452 (Dautzenberg, 1989)

Step 6: Calculate minimum L/d_P

$L/d_p > 92 * 10.71^{-0.23} * 1 * \ln(1/(1-0.5)) = 36.96$

In our case, L/dp = 270 (Dautzenberg, 1989)

Hence, the condition is satisfied for plug flow

Verification of absence of mass and heat transfer limitations: detailed calculations of criteria

Catayst 2 - Example of detailed calculations of criteria to confirm the absence of mass and heat transfer limitations at 350 ° C in the wet (10 vol%) feed for the Pd-Pt/10Co/SnO_2 catalyst and 5000 ppmv methane concentration. Since the catalyst is non-porous internal mass and heat transfer limitations do not exist.

Parameter	Equation	Value (calculated or experimental)
Reaction rate - r_M, [mol/(s·kg_{cat})]	$-r_M = \frac{F_{Mo}X}{W}$	**2.31×10^{-4}** For initial methane molar flow rate $F_{Mo} = 7.86 \times 10^{-7}$ mol/s, catalyst amount W = 0.34 g, conversion at differential conditions X = 0.1
Methane bulk diffusivity in air	$D_{AB} = \frac{1.013 \cdot 10^{-2} T^{1.75} \left[\frac{1}{M_A} + \frac{1}{M_B}\right]^{0.5}}{P\left[\left(\sum \nu_i\right)_A^{1/3} + \left(\sum \nu_i\right)_B^{1/3}\right]^2}$	**7.82×10^{-5}** For P =101325 Pa, molecular masses and diffusion volumes for

at 623.15 K D_{AB} [m^2/s]	(Fuller formula (Fuller et al., 1966; Hayes and Mmbaga, 2012))	methane and air as 16 g/mol, 29 g/mol, 24.42, and 20.1 (Fuller et al., 1966; Hayes and Mmbaga, 2012)
Particle Reynolds number Re_P	$\mathrm{Re} = \frac{U\rho_g d_p}{\mu}$ (Fogler, 2011)	**0.0772** For dynamic viscosity $\mu = 3.4\times10^{-5}$ Pa·s [1] and density r = 0.5247 kg/m^3 (ideal gas) of air at 623.15 K [7] , $d_p = 5\times10^{-5}$ m, free-stream velocity 0.1 m/s (for 3/8" reactor ID and assuming bed porosity of 0.4)
Schmidt number	$\mathrm{Sc} = \frac{\mu}{D_{AB}\rho_g}$ (Fogler, 2011)	**0.829**
Sherwood number Sh	$\mathrm{Sh} = 2 + 0.6\mathrm{Re}^{1/2}\mathrm{Sc}^{1/3}$ (Frössling correlation (Fogler, 2011))	**2.16**
Mass transfer coefficient k_c [m/s]	$k_c = \frac{D_{AB}\mathrm{Sh}}{d_p}$ (Fogler, 2011)	**3.37**
Mears criterion for external diffusion	$\frac{-r_M\rho_b\mathrm{Rn}}{k_c C_M} < 0.15$ If the condition is satisfied, then no external MTL is present (Fogler, 2011)	**3.36×10^{-5}** For ϱ_b (bed density) 3954 kg/m^3 (catalyst density ϱ_c 6590 kg/m^3, bed porosity 0.4), particle radius R = 2.5×10^{-5} m, order n = 1, $C_M = C_{Mo}(1\text{-}X)$ with initial methane concentration of 0.2025 mol/m^3
Thus, the Mears criterion shows the absence of external mass transfer limitations		
Nusselt number Nu	$\mathrm{Nu} = 2 + 0.6\mathrm{Re}^{1/2}\mathrm{Pr}^{1/3}$ (Fogler, 2011)	**2.15** For Prandtl number Pr = 0.683 for air at 623.15 K (Dry Air Properties)

Heat transfer coefficient h [kJ/(m²·s·K)]	$h = \frac{k_t Nu}{d_p}$ (Fogler, 2011)	**2.18** For thermal conductivity of air at 623.15 K as 0.03365 W/(m·K) (Dry Air Properties)
External temperature gradient criterion	$\left\lvert \frac{-r_M(-\Delta H_{rx})\rho_b RE}{hT^2 R_{gas}} \right\rvert < 0.15$ If the condition is satisfied, then no external HTL are present (Fogler, 2011)	**3.18×10^{-4}** For the heat of reaction -890 kJ/mol and activation energy E 110 kJ/mol (as reported in Table 2)
Thus, the external temperature gradient criterion shows the absence of external HTL		
All the criteria above confirm that the reaction at 350 °C occurs in the kinetic regime and that the ideal PBR mole balance is applicable		

Catalyst 3 - The kinetic regime was verified at 400 °C in the wet (10 vol%) feed for the Pd-Pt/SnO_2 catalyst and 4000 ppmv methane concentration. Since the catalyst is non-porous internal mass and heat transfer limitations do not exist.

Parameter	Equation	Value (calculated or experimental)
Reaction rate - r_M, [mol/(s·kg_{cat})]	$-r_M = \frac{F_{Mo}X}{W}$	**1.86×10^{-8}** For initial methane molar flow rate $F_{Mo} = 1.58 \times 10^{-7}$ mol/s, catalyst amount W = 0.34 g, conversion at differential conditions X = 0.04
Methane bulk diffusivity in air at 673.15 K D_{AB} [m^2/s]	$D_{AB} = \frac{1.013 \cdot 10^{-2} T^{1.75} \left[\frac{1}{M_A} + \frac{1}{M_B}\right]^{0.5}}{P\left[\left(\sum \nu_i\right)_A^{1/3} + \left(\sum \nu_i\right)_B^{1/3}\right]^2}$ (Fuller formula (Fuller et al., 1966; Hayes and Mmbaga, 2012))	**8.95×10^{-5}** For P =101325 Pa, molecular masses and diffusion volumes for methane and air as 16 g/mol, 29 g/mol, 24.42, and 20.1 (Fuller et al., 1966; Hayes and Mmbaga, 2012)
Particle Reynolds number Re_P	$Re = \frac{U\rho_g d_p}{\mu}$ (Fogler, 2011)	**0.033** For dynamic viscosity $\mu = 3.4 \times 10^{-5}$ Pa·s (Lyons et al., 2016) and density = 0.5247 kg/m^3 (ideal gas) of air at 673.15 K ("Dry Air Properties," n.d.) , $d_p = 5 \times 10^{-5}$ m, free-stream velocity 0.04266 m/s (for 3/8" reactor ID and assuming bed porosity of 0.4)
Schmidt number	$Sc = \frac{\mu}{D_{AB}\rho_g}$ (Fogler, 2011)	**0.72**
Sherwood number Sh	$Sh = 2 + 0.6Re^{1/2}Sc^{1/3}$ (Frössling correlation (Fogler, 2011))	**2.10**

Mass transfer coefficient k_c [m/s]	$k_c = \frac{D_{AB} Sh}{d_p}$ (Fogler, 2011)	**3.76**
Mears criterion for external diffusion	$\frac{-r_M \rho_b Rn}{k_c C_M} < 0.15$ If the condition is satisfied, then no external MTL is present (Fogler, 2011)	**$1{\cdot}14 \times 10^{-8}$** For ρ_b bed density 3954 kg/m^3 (catalyst density ρ_c 6590 kg/m^3, bed porosity 0.4), particle radius R = 2.5×10^{-5} m, order n = 1, $C_M = C_{Mo}(1\text{-}X)$ with initial methane concentration of 0.0451 mol/m^3
Thus, the Mears criterion shows the absence of external mass transfer limitations		
Nusselt number Nu	$Nu = 2 + 0.6Re^{1/2}Pr^{1/3}$ (Fogler, 2011)	**2.10** For Prandtl number Pr = 0.708 for air at 673.15 K ("Dry Air Properties," n.d.)
Heat transfer coefficient h [kJ/(m^2·s·K)]	$h = \frac{k_t Nu}{d_p}$ (Fogler, 2011)	**2.13** For thermal conductivity of air at 673.15 K as 0.0508 W/(m·K) ("Dry Air Properties," n.d.)
External temperature gradient criterion	$\left\lvert \frac{-r_M(-\Delta H_{rx})\rho_b RE}{hT^2 R_{gas}} \right\rvert < 0.15$ If the condition is satisfied, then no external HTL are present (Fogler, 2011)	**2.03×10^{-13}** For the heat of reaction -890 kJ/mol (Abbasi et al., 2012) and activation energy E = 127.9 kJ/mol
Thus, the external temperature gradient criterion shows the absence of external HTL		
All the criteria above confirm that the reaction at 400 °C occurs in the kinetic regime and that the ideal PBR mole balance is applicable		

Catalyst 5 - Example of detailed calculations of criteria to confirm the absence of mass and heat transfer limitations at 350 ° C in the wet (10 vol%) feed for the Pd-Pt/10Co/ γ-Al_2O_3 catalyst and 5000 ppmv methane concentration.

Parameter	Equation	Value (calculated or experimental)
Reaction rate - r_M, [mol/(s·kg_{cat})]	$-r_M = \frac{F_{Mo}X}{W}$	**1.16×10^{-4}** For initial methane molar flow rate F_{Mo} = 7.86×10^{-7} mol/s, catalyst amount W = 0.34 g, conversion at differential conditions X = 0.05
Methane bulk diffusivity in air at 623.15 K D_{AB} [m^2/s]	$D_{AB} = \frac{1.013 \cdot 10^{-2} T^{1.75} \left[\frac{1}{M_A} + \frac{1}{M_B}\right]^{0.5}}{P\left[\left(\sum \nu_i\right)_A^{1/3} + \left(\sum \nu_i\right)_B^{1/3}\right]^2}$ (Fuller formula (Fuller et al., 1966; Hayes and Mmbaga, 2012))	**7.82×10^{-5}** For P =101325 Pa, molecular masses and diffusion volumes for methane and air as 16 g/mol, 29 g/mol, 24.42, and 20.1 (Fuller et al., 1966; Hayes and Mmbaga, 2012)
Particle Reynolds number Re_p	$Re = \frac{U\rho_g d_p}{\mu}$ (Fogler, 2011)	**0.0772** For dynamic viscosity μ = 3.4×10^{-5} Pa·s [1] and density r = 0.5247 kg/m^3 (ideal gas) of air at 623.15 K [7] , d_p = 5×10^{-5} m, free-stream velocity 0.1 m/s (for 3/8″ reactor ID and assuming bed porosity of 0.4)
Schmidt number	$Sc = \frac{\mu}{D_{AB}\rho_g}$ (Fogler, 2011)	**0.829**
Sherwood number Sh	$Sh = 2 + 0.6Re^{1/2}Sc^{1/3}$ (Frössling correlation (Fogler, 2011))	**2.16**
Mass transfer coefficient k_c [m/s]	$k_c = \frac{D_{AB}Sh}{d_p}$ (Fogler, 2011)	**3.37**
Mears criterion for external diffusion	$\frac{-r_M \rho_b Rn}{k_c C_M} < 0.15$ If the condition is satisfied, then no external MTL is present (Fogler, 2011)	**3.68×10^{-6}** For catalyst density ϱ_c = $1/((1/\varrho_s)+V_0)$ = 1524.23 kg/m^3 [8]; where ϱ_s is solid density = 3890 kg/m^3 and V_0 is pore volume =

		0.399 cc/g (bed density ϱ_b = 914.537 kg/m^3, (bed porosity 0.4), particle radius R = 2.5 × 10^{-5} m, order n = 1, $C_M = C_{Mo}(1-X)$ with initial methane concentration of 0.213 mol/m^3
Thus, the Mears criterion shows the absence of external mass transfer limitations		
Knudsen diffusivity [m^2/s]	$D_K = \frac{d_{pore}}{3}\sqrt{\frac{8RT}{\pi M}}$ (Hayes and Mmbaga, 2012)	**1.30 × 10^{-6}** For methane (molecular mass M 0.016 kg/mol) and catalyst pore diameter d_{pore} = 4.31 nm (Figure S3b)
Diffusivity in a pore [m^2/s]	$D_{pore} = \left(\frac{1}{D_{AB}} + \frac{1}{D_K}\right)^{-1}$ (Hayes and Mmbaga, 2012)	**1.28 × 10^{-6}**
Particle porosity	$\phi_p = \frac{S\rho_c\, d_{Pore}}{4}$ (Hayes and Mmbaga, 2012)	**0.1971** For catalyst surface area S = 120 m^2/g (Figure S3a)
Effective diffusivity [m^2/s]	$D_{eff} = \frac{\phi_P D_{pore}}{\tau}$ (Hayes and Mmbaga, 2012)	**6.47 × 10^{-8}** For tortuosity 3.9
Weisz-Prater criterion for internal MTL	$C_{WP} = \frac{-r_M \rho_c R^2}{D_{eff} C_M}$ If $C_{WP} < 0.3$ for a first-order reaction, then no internal MTL is present (Fogler, 2011)	**8.00 × 10^{-3}** For C_M as the bulk concentration of 0.213 mol/m^3 since the absence of external MTL was proved
Thus, the Weisz-Prater criterion shows the absence of internal mass transfer limitations		
Nusselt number Nu	$Nu = 2 + 0.6Re^{\frac{1}{2}}Pr^{\frac{1}{3}}$ (Fogler, 2011)	**2.15** For Prandtl number Pr = 0.683 for air at 623.15 K [7]
Heat transfer coefficient h [kJ/(m^2·s·K)]	$h = \frac{k_t Nu}{d_p}$ (Fogler, 2011)	**2.18** For thermal conductivity of air at 623.15 K as 0.03365 W/(m·K) [7]

External temperature gradient criterion	$\left\|\frac{-r_M(-\Delta H_{rx})\rho_b RE}{hT^2 R_{gas}}\right\| < 0.15$ If the condition is satisfied, then no external HTL are present (Fogler, 2011)	**4.44×10^{-5}** For the heat of reaction -890 kJ/mol and activation energy E 133 kJ/mol (as reported in Table 2)
Thus, the external temperature gradient criterion shows the absence of external HTL		
Prater number b	$\beta = \frac{-H_{rxn} D_{eff} C_M}{k_{eff} T}$ (Hayes and Mmbaga, 2012)	**5.62×10^{-7}** For effective thermal conductivity of Al_2O_3 as 0.035 kW/(m·K) [10]
Maximum internal temperature rise [K]	$\Delta T_{max} = \beta T$ (Hayes and Mmbaga, 2012)	**3.50×10^{-4}** The maximum internal T can be 623.15 K which is the same as 623.15 K surface. The catalyst particle is thus isothermal
Thus, the Prater number shows the absence of internal HTL		
All the criteria above confirm that the reaction at 350 ˚C occurs in the kinetic regime and that the ideal PBR mole balance is applicable		

Catalyst 6 - The kinetic regime was verified at 400 ˚C in the wet (10 vol%) feed for the Pd-Pt/γ-Al_2O_3 catalyst and 4000 ppmv methane concentration.

Parameter	Equation	Value (calculated or experimental)
Reaction rate - r_M, [mol/(s·kg_{cat})]	$-r_M = \frac{F_{Mo} X}{W}$	**2.3×10^{-8}** For initial methane molar flow rate F_{Mo} = 1.58 × 10^{-7} mol/s, catalyst amount W = 0.34 g, conversion at differential conditions X = 0.05
Methane bulk diffusivity in air at 613 K D_{AB} [m^2/s]	$D_{AB} = \frac{1.013 \cdot 10^{-2} T^{1.75} \left[\frac{1}{M_A} + \frac{1}{M_B}\right]^{0.5}}{P\left[(\sum \nu_i)_A^{1/3} + (\sum \nu_i)_B^{1/3}\right]^2}$	**8.95×10^{-5}** For P =101325 Pa, molecular masses and diffusion volumes for methane and air as 16 g/mol, 29 g/mol, 24.42,

	(Fuller formula (Fuller et al., 1966; Hayes and Mmbaga, 2012))	and 20.1 (Fuller et al., 1966; Hayes and Mmbaga, 2012)
Particle Reynolds number Re_p	$Re = \frac{U\rho_g d_p}{\mu}$ (Fogler, 2011)	**0.033** For dynamic viscosity μ = 3.4×10^{-5} Pa·s (Lyons et al., 2016) and density = 0.5247 kg/m^3 (ideal gas) of air at 673.15 K ("Dry Air Properties," n.d.) , d_p = 5×10^{-5} m, free-stream velocity 0.04266 m/s (for 3/8" reactorID and assuming bed porosity of 0.4)
Schmidt number	$Sc = \frac{\mu}{D_{AB}\rho_g}$ (Fogler, 2011)	**0.72**
Sherwood number Sh	$Sh = 2 + 0.6Re^{1/2}Sc^{1/3}$ Frössling correlation (Fogler, 2011)	**2.10**
Mass transfer coefficient k_c [m/s]	$k_c = \frac{D_{AB}Sh}{d_p}$ (Fogler, 2011)	**3.76**
Mears criterion for external diffusion	$\frac{-r_M\rho_b Rn}{k_c C_M} < 0.15$ If the condition is satisfied, then no external MTL is present (Fogler, 2011)	**8.42×10^{-9}** For $_b$ bed density 2334 kg/m^3 (catalyst density $_c$ 3890 kg/m^3, bed porosity 0.4), particle radius R = 2.5×10^{-5} m, order n = 1, $C_M = C_{Mo}(1-X)$ with initial methane concentration of 0.0451 mol/m^3
Thus, the Mears criterion shows the absence of external mass transfer limitations		
Knudsen diffusivity [m^2/s]	$D_K = \frac{d_{pore}}{3}\sqrt{\frac{8RT}{\pi M}}$ (Hayes and Mmbaga, 2012)	**1.86×10^{-7}** For methane (molecular mass M 0.016 kg/mol) and catalyst pore diameter d_{pore} = 0.59 nm (specified by Sigma-Aldrich)

Diffusivity in a pore [m^2/s]	$D_{pore} = \left(\frac{1}{D_{AB}} + \frac{1}{D_K}\right)^{-1}$ (Hayes and Mmbaga, 2012)	**1.87×10^{-7}**
Particle porosity	$\phi_p = \frac{S\rho_c\, d_{Pore}}{4}$ (Hayes and Mmbaga, 2012)	**0.028** For catalyst surface area 155 m^2/g and catalyst density 3890 kg/m^3 (specified by Sigma-Aldrich)
Effective diffusivity [m^2/s]	$D_{eff} = \frac{\phi_P D_{pore}}{\tau}$ (Hayes and Mmbaga, 2012)	**1.34×10^{-9}** For tortuosity 3.9
Weisz-Prater criterion for internal MTL	$C_{WP} = \frac{-r_M \rho_c R^2}{D_{eff} C_M}$ If $C_{WP} < 0.3$ for a first-order reaction, then no internal MTL is present (Fogler, 2011)	**9.70×10^{-4}** For C_M as the bulk concentration of 0.043 mol/m^3 since the absence of external MTL was proved
Thus, the Weisz-Prater criterion shows the absence of internal mass transfer limitations		
Nusselt number Nu	$Nu = 2 + 0.6 Re^{\frac{1}{2}} Pr^{\frac{1}{3}}$ (Fogler, 2011)	**2.10** For Prandtl number Pr = 0.688 for air at 673.15 K ("Dry Air Properties," n.d.)
Heat transfer coefficient h [$kJ/(m^2 \cdot s \cdot K)$]	$h = \frac{k_t Nu}{d_p}$ (Fogler, 2011)	**2.13** For thermal conductivity of air at 673.15 K as 0.03365 W/(m·K) ("Dry Air Properties," n.d.)
External temperature gradient criterion	$\left\lvert\frac{-r_M(-\Delta H_{rx})\rho_b RE}{hT^2 R_{gas}}\right\rvert < 0.15$ If the condition is satisfied, then no external HTL are present (Fogler, 2011)	**1.92×10^{-11}** For the heat of reaction -890 kJ/mol and activation energy E 129.1 kJ/mol (as reported in Table 2)
Thus, the external temperature gradient criterion shows the absence of external HTL		
Prater number	$\beta = \frac{-H_{rxn} D_{eff} C_M}{k_{eff} T}$ (Hayes and Mmbaga, 2012)	**1.68×10^{-4}**

		For effective thermal conductivity of Al_2O_3 as 0.043 W/(m·K) (Mürtezaoğlu et al., 1995)
Maximum internal temperature rise [K]	$\Delta T_{max} = \beta T$ (Hayes and Mmbaga, 2012)	**0.11** The maximum internal T can be 673.26 K instead of 673.15 K surface. The catalyst particle is thus isothermal
Thus, the Prater number shows the absence of internal HTL		
All the criteria above confirm that the reaction at 400 °C occurs in the kinetic regime and that the ideal PBR mole balance is applicable		

References

Dautzenberg, F.M., 1989. Ten Guidelines for Catalyst Testing 99–119. https://doi.org/10.1021/bk-1989-0411.ch011

Dry Air Properties [WWW Document], n.d. URL https://www.engineeringtoolbox.com/dry-air-properties-d_973.html

Fogler, S., 2011. Elements of Chemical Reaction Engineering, 5th ed.

Fuller, E.N., Schettler, P.D., Giddings, J.C., 1966. A new method for prediction of binary gas-phase diffusion coefficients. Ind. Eng. Chem. 58, 18–27. https://doi.org/10.1021/ie50677a007

Hayes, R.E., Mmbaga, J.P., 2012. Introduction to chemical reactor analysis, second edition, 2nd ed, Introduction to Chemical Reactor Analysis, Second Edition. Taylor and Francis Group, CRC Press.

Lyons, W., Plisga, G., Lorenz, M., 2016. Standard handbook of petroleum and natural gas engineering, 3rd ed. Elsevier.